"Instrumentation Engineering, Electronics and Telecommunications – 2017"

Proceedings of the III International Forum

November 22–24, 2017
Izhevsk, Russia

«ПРИБОРОСТРОЕНИЕ, ЭЛЕКТРОНИКА И ТЕЛЕКОММУНИКАЦИИ – 2017»

Сборник статей III Международного форума

(Ижевск, Россия, 22–24 ноября 2017 г.)

УДК 681.2(06)

На обложке использована фотография Ildefonso Polo из фотостока Unsplash

Сборник содержит прошедшие рецензирование статьи на английском языке по широкому кругу вопросов в областях приборостроения, электроники, связи и смежных им, которые обсуждались на III Международном форуме «Instrumentation Engineering, Electronics and Telecommunications – 2017» («Приборостроение, электроника и телекоммуникации – 2017»), проводимом в рамках XIII Международной научно-технической конференции «Приборостроение в XXI веке. Интеграция науки, образования и производства» (22–24 нояб. 2017 г., Ижевск, Россия).

Материалы статей могут быть полезны ученым, специалистам, молодым исследователям, аспирантам и студентам.

УДК 681.2(06)

"INSTRUMENTATION ENGINEERING, ELECTRONICS AND TELECOMMUNICATIONS – 2017"

Proceedings of the III International forum

(Izhevsk, Russia, November 22–24, 2017)

UDC 681.2(06)

Organizing Committee Chairmans

Scientific Committee (Peer Reviewers)

Editorial Board

Photo on the cover by Ildefonso Polo on Unsplash

TABLE OF CONTENTS

Collision Free 3D Navigation Algorithms and Their Implementation in an Autonomous Flying Robot

I. N. Ibrahim [1], A. A. Karam [2], M. A. Al Akkad [3]

[1] Department of Mechatronics, Kalashnikov Izhevsk State Technical University,
Izhevsk, Russian Federation
E-mail: ibrncfe@gmail.com
[2] Department of Mechatronics Engineering, University of Tehran,
Tehran, Iran
E-mail: k.maghout@gmail.com
[3] Department of Computer Science, Kalashnikov Izhevsk State Technical University,
Izhevsk, Russian Federation
E-mail: aimanakkad@yandex.ru

Abstract. In this paper, a method for collision-free three-dimensional autonomous navigation of an underactuated coupled non-holonomic unmanned aerial vehicle (UAV) among obstacles was proposed. This method will be the basis for designing a planner for the UAV trajectory guidance in a 3D cluttered environment. The planner assumes that the cost of flying over an area is independent of the path through which the UAV reaches that area, however this is not always true. Moreover, the path problem is not formulated as a matter of numeric cost minimization to be solved by methods like dynamic programming, which is time-consuming. A dynamic model of six degrees of freedom hexacopter equipped with a robotic arm has been formulated using Newton-Euler's method. Then, the equations of motion of the UAV are derived by including disturbances analysis. The derived dynamic model reflects the real motion of the hexacopter with respect to the earth, which is also characterized by nonlinearity, time variance, underactuation and coupling among the equations' variables. This paper suggests bio-inspired and sample-based algorithms in order to solve and optimize the three-dimensional path-planning problem. A unique real-time obstacle avoidance approach based on artificial potential field concept in addition to an off-line genetic algorithm were investigated.

INTRODUCTION

Tsai, et al. [1] proposed a three-dimensional real-time path planning based on rapidly-exploring random tree algorithm (RRT). However, the paths generated are, in general, not optimal due to the existence of redundant waypoints. Bagheran and Alos [2] used genetic algorithm (GA) and particle swarm algorithms to generate the path that should be a sequence of speed rate and angles at discrete times, where the cost function was calculated precisely and 3D maps were generated containing the geographic data accompanied by a digital terrain model and a geographical information system. Two approaches were investigated the artificial

potential field algorithm (APF) and the genetic algorithm (GA). APF algorithms are sorted as sampling-based algorithm because it needs the whole workspace sampling information to escape from local minima [3]. While genetic algorithm [4–5] is the most famous population-based numerical optimization method and originate from mimicking biological behavior in solving problems, Gouda [4] presented a path planning for a manipulator in a 3D environment based on a GA method, where the full and optimized path was formulated as three real chromosomes containing three-real trajectories in a fixed time. Zhang, et al. [5] proposed fuzzy logic control technology to solve the distance between the vessels to solve uncertainty-planning problem of a set of underactuated unmanned vehicles within a given space, moreover, they used GA to optimize the input/output scaling factor of a fuzzy controller. Interesting ideas for path formulation in addition to fuzzy adaptive differential evolution for path planning in a 3D environment was presented in [6–9], where UAV must have some sensing capabilities to operate in a dynamic environment while it is not required in a static environment as every information of the environment will be known beforehand. Wang and Zhang [10] used a fuzzy logic approach as a method to output a threat cost gain in order to enable the UAV escape from a sudden threat quickly, and the final route was calculated by a differential evolution algorithm. Shen, et al. [11] used a model predicting technique in real-time to find an optimal track in a three-dimensional complex environment, especially under the threat of moving targets. Where the weight of each factor of maneuvering performance was calculated by a multi-objective optimization algorithm in the search space. Kurnaz, et al. [12] used tactical air navigation (TACAN) approach and the performance of the fuzzy based controllers is evaluated with time-based diagrams, the simulation studies presented verify that the UAV can follow the predefined trajectories despite the simplicity of the controllers. Kurnaz, et al. [13] evaluated the performance of adaptive neuro-fuzzy inference system (ANFIS) based controllers in relation to the autonomous operation of UAVs, nevertheless, for some flight conditions, the ANFIS type controller has resulted in unstable performance. This has demonstrated that more stable learning algorithms need to be adopted. Vadakkepat, et al. [14] used an APF method combined with a genetic algorithm, to derive a new methodology named evolutionary artificial potential field (EAPF), the proposed method aims to navigate robots situated among moving obstacles based on optimal potential field functions. Khatib [15] proposed APF as a real-time obstacle avoidance approach for manipulators and mobile robots. APF methods have lower computational requirements than local planning approaches and could be extended to moving obstacles by using time-varying and adaptive techniques while running [16]. Wang, et al. [17] extended the range of robot's vision in order to operate in unknown and uncertain dynamic three-dimensional environments with a number of stationary or moving obstacles. Lee, et al. [18] addressed a new inherent limitation of the potential field methods referred to as symmetrically aligned robot-obstacle-goal (SAROG), which involves critical risk of local minima trap.

PROBLEM STATEMENT

This paper suggests a design of a robot guidance algorithm, which will be used as a planner for UAV navigation with collision avoidance in a 3D cluttered environment. This design is based on bio-inspired and sampling-based algorithms with two types of known 2D-3D environments. This problem of path planning is attributed to the top layer of a robot control process. And it is described as a continuous real-time planning, in a dynamic 3D environment with a number of stationary or moving obstacles, of a non-holonomic under-actuated nonlinear UAV with bounded control input.

We suggest that the vehicle operates in a three-dimension (R^3) space called S as shown in Figure 1 that contains several static and dynamic obstacles Os_i and Od_i. Obstacles can be of any irregular shapes but we assume that obstacles are always inside or covered by a sphere of a known radius r_i and a known center c_i located in obstacle space called $S_{obstacle}$. In addition, there is also a stationary start point S and a target point T located in a three-dimensional free space called S_{free}. Now the objective is to generate trajectories of the path from S to T in S_{free} where the vehicle should always stay. Thus, the path-planning problem is defined by a triplet (S, T, S_{free}), with the following definitions [3]:

– **Path planning** is a continuous unbreakable process F that achieves $\delta(\tau) \in S_{free}$, for all $\tau \in [0, L]$ where $\delta \subset R^3$ is a function of bounded variation, where $\delta(0) = S$ and $\delta(L) = T$.

– **Optimal path planning** is a process F^* after fulfilling F to find the optimal path δ^* whose cost is $\min(C(\delta_i))$, where δ_i is the set of all feasible paths, and C is the cost function:

$$\sum_i C(\delta_i) \in R \,\big|\, \delta_i \geq 0.$$

– **Path planning augmentation** is the process of finding a continuous curve in the configuration space made up of segments of which each can be a trajectory, and starts at node S and ends at node T, without continuous time consideration, including stops in defined position.

– **Trajectory generation** is the process of taking the solution from the path planning algorithm and determining how to move along the path, considering the Kino dynamic constraints, which can be an element of the path. The trajectory is a set of states that are associated with time, described by a polynomial $X(t)$. Velocities and accelerations are computed by taking derivatives with respect to time.
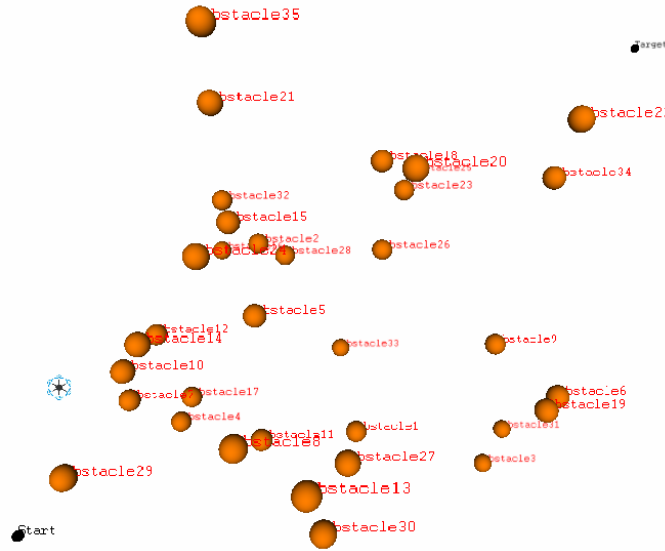
Figure 1. Three-dimension (R^3) environment

METHODOLOGY PATH FORMULATION

In this initial path planning research, it is assumed that all the information about the environment, including the obstacles' areas, is known to the UAV. In our study, the UAV is assumed to be in an environment with different obstacles' areas. The UAV has to avoid the obstacles areas; otherwise, there will be some penalty for paths passing through those areas. The

path-planning problem can also be formulated as a 3D path-planning problem or a 2D path-planning problem, by assuming the constant altitude sometime after takeoff. All three dimensions are considered in this study during the entire flight [4]. The main goals in our method are to produce an optimum 3D path by taking into our consideration real-time computational time, obstacles areas and path distance from S to T while formulating the path. Figure 2 shows Voronoi diagram that was introduced by Shamos and Hoey [45] and developed by Luchnikov et al. [44] for 3D environments. It is used to generate the topological connection. With high number of obstacles the problem turns out sophisticated and here we can see if there is a solution based on the calculation of the Voronoi channel [45]. Figure 2 demonstrates the complexity of the problem for a fixed altitude.
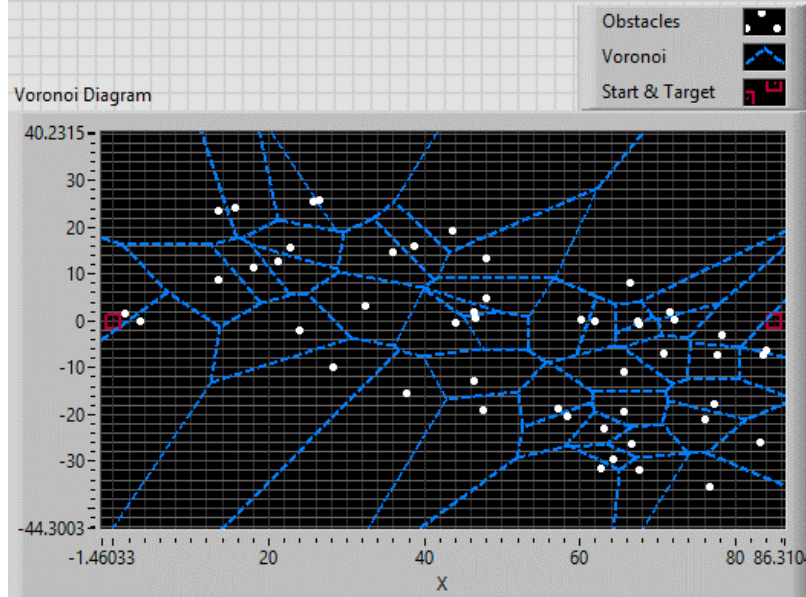
Figure 2. Voronoi diagram of environment

In this paper, two types of algorithms will be investigated: artificial potential field algorithm in the 3D environment and bio-inspired algorithms in the 2D environment after assuming the constant altitude. Firstly, the initial path process is initialized by determining the start point S and the target point T, as shown in Figure 3. There are some obstacles' areas in the task region, which are all presented in the form of a sphere. In this environment, we will apply APF algorithm which works on-line, while the vehicle is in the space, by taking only the coordinates, the center, and the radius of each obstacle. Then we will apply bio-inspired algorithms (genetic and differential evolution algorithms) which works off-line after doing some transformations in the 2D environment.

These simplifications are as follow. First, we connect point S and point T in a straight line, which is considered as the optimum path but contains penalty collisions with obstacles, so we divide this line to equal ST segments that define the accuracy of the planning, draw a vertical line of at each ST segment point. This set of lines can be denoted as $L_1, L_2, ..., L_k, ..., L_T$ at each line producing a discrete points collection

$$C_k = \left\{ ..., \left(x(k), y(i-2) \right), \left(x(k), y(i-1) \right), \left(x(k), y(i) \right), \left(x(k), y(i+1) \right), \left(x(k), y(i+2) \right), ... \right\},$$

which is called waypoint. We take a discrete waypoint at each line and connect them in sequence form in a flight path P. In this way, the path-planning problem is turning into optimizing the coordinate series to achieve a superior fitness value of the objective function. To ac-

celerate the algorithm's search speed, we can let ST line be the *X*-axis and take the coordinate transformation on each discrete point $(x(k), y(k))$ according to formula (1), as shown in Figure 3, where $(-\pi < \theta < \pi)$ is the angle that the original *X*-axis counterclockwise rotates to parallel ST segment, while (x_s, y_s) represent the coordinates in the original coordinate system [5–6, 9]. Figure 4 shows the problem of path planning after applying the simplifications with fixed radius obstacles:

$$\begin{bmatrix} X' \\ Y' \end{bmatrix} = R_\theta \begin{bmatrix} X \\ Y \end{bmatrix}, \text{ while } R_\theta = \begin{bmatrix} \cos\theta & \sin\theta \\ -\sin\theta & \cos\theta \end{bmatrix}. \tag{1}$$
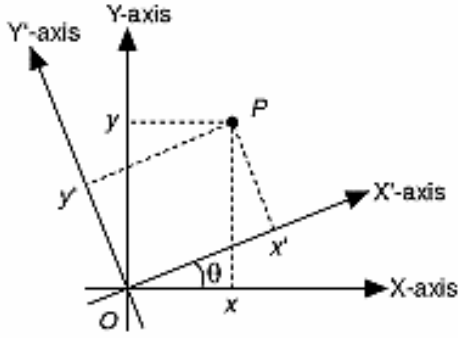
Figure 3. Rotation of a two-dimensional Cartesian coordinate
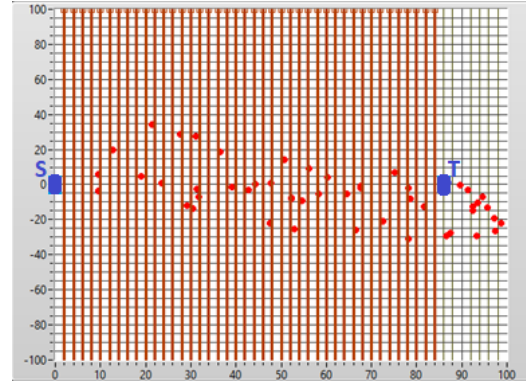
Figure 4. Path planning formulation and coordinate transformation

UAV EQUATIONS OF MOTION

In this paper the flight model equations and UAV physical constraints are similar to [21, 22]. A simplified kinematics model of a UAV flying in a three-dimensional airspace is of interest. So, the UAV is considered as a point in a 3D space, and its translational and angular states at time *t* are defined in [23–25] as follow:

$$\begin{bmatrix} \ddot{x} \\ \ddot{y} \\ \ddot{z} \end{bmatrix} = \begin{bmatrix} U_x \\ U_y \\ U_z - g \end{bmatrix} + \begin{bmatrix} \dfrac{F_{dI_x}}{m} \\ \dfrac{F_{dI_y}}{m} \\ \dfrac{F_{dI_z}}{m} \end{bmatrix}, \text{ where } \begin{cases} U_x = (c\phi c\psi s\theta + s\phi s\psi)u_T / m, \\ U_y = (c\phi s\psi s\theta - s\phi c\psi)u_T / m, \\ U_z = (c\phi c\theta)u_T / m. \end{cases} \tag{2}$$

The inertial frame position of the vehicle is given by vector $\xi = [x \ \ y \ \ z]^T$. The angular position of the body frame with respect to the inertial one is usually defined by means of the Euler angles: roll ϕ, pitch θ, and yaw ψ where $c\theta$ is equivalent to $\cos\theta$, also $s\theta$ means $\sin\theta$, and so on, *g* is the gravity acceleration, *m* is the mass of aircraft, the disturbance force is the other forces like Coriolis force from the earth, wind, and Euler forces which are considered as disturbances, summarized as F_{DI} in the Earth frame: $F_{DI} = [F_{dIx} \ \ F_{dIy} \ \ F_{dIz}]^T_E$, blade

rotation is with angular velocity ω. Finally, the total thrust force vector of the aircraft is u_T and it is the sum of the propellers thrust force vectors $\sum\limits_{i=1}^{6} T_i$.

OBJECTIVE FUNCTIONS

UAV path planning is generally formulated as a multi-objective optimization problem. The most critical objective is the path length, which can be directly translated to energy and obstacle costs along the path. However, there are researches that take the objectives [2, 6, 27]. In our study, the UAV path planning is considered as a bi-objective optimization problem in the aim of minimization of both energy cost and obstacle cost. The energy cost J_e is directly dependent on the path length P by measuring the distance from a specified waypoint to the target while obstacle cost J_o represents the distance from each center of an obstacle by taking into account the radius of the obstacle, as follows:

$$J_e = \int_0^P w_e dt, \quad J_o = \int_0^P w_o dt. \tag{3}$$

Where w_e, w_o are the weights for UAV for the whole path. This research focuses on two methods for finding a solution and optimization, the artificial potential field and the genetic algorithm methods. The first one is an active classical approach of sampling-based algorithms to reactive collision avoidance. This method depends on three objective functions that cause repelling from obstacles and attraction to the target, in addition to, escaping from local minima trap [18–20]. Then weight functions can be now written in 3D workspace as follows:

$$w_e = \begin{cases} 0, & \text{if UAV at the Target,} \\ \alpha\left[(x_{target} - x_{uav})^2 + (y_{target} - y_{uav})^2 + (z_{target} - z_{uav})^2\right], & \text{otherwise,} \end{cases} \tag{4}$$

$$w_o = \begin{cases} 0, & \text{if collision free,} \\ \dfrac{\varepsilon}{\sum\limits_{t=1}^{m}\left[(x_{obstacle_t} - x_{uav})^2 + (y_{obstacle_t} - y_{uav})^2 + (z_{obstacle_t} - z_{uav})^2\right]}, & \text{otherwise,} \end{cases} \tag{5}$$

where m is the number of obstacles in the workspace, α and ε are the attractive and repulsive parameters respectively, $\begin{bmatrix} x_{uav} & y_{uav} & z_{uav} \end{bmatrix}^T$ is the UAV coordination's vector, $\begin{bmatrix} x_{target} & y_{target} & z_{target} \end{bmatrix}^T$ is the target coordinate's vector and $\begin{bmatrix} x_{obstacle_t} & y_{obstacle_t} & z_{obstacle_t} \end{bmatrix}^T$ is the tth obstacle coordinate's vector.

While the other algorithm is the genetic algorithm which is the second method discussed in this study, this is one of the bio-inspired algorithms that aims to optimize the problem based on objective cost. Like previous methods, two parameters were also analyzed in this study, distance to the target and to the obstacles. Then weight equations can be written as extended forms for each waypoint i in the vertical line of segment k and n is a number of waypoints in each level k, as follows:

$$J_{ek} = \sum_{i=1}^{n} D_{eik}^{\ 2}, \tag{6}$$

$$J_{ok} = \sum_{t=1}^{m} \sum_{i=1}^{n} \frac{1}{D_{o_{t,ik}}{}^2}, \tag{7}$$

$$D_{eik} = \sqrt{(x_{target} - x_{uav_{ik}})^2 + (y_{target} - y_{uav_{ik}})^2}, \tag{8}$$

$$D_{o_{t,ik}} = \sum_{t=1}^{m} \sqrt{(x_{obstacle_t} - x_{uav_{ik}})^2 + (y_{obstacle_t} - y_{uav_{ik}})^2}. \tag{9}$$

ARTIFICIAL POTENTIAL FIELD METHOD

The philosophy of artificial potential field method APF can be schematically described by the movement of the vehicle in a field of forces. The position to be reached is an attractive pole for the target and the obstacles are repulsive forces for the vehicles [42] as shown in Figure 5. In addition to, an escape force for the critical risk of local minima trap, which is a new inherent limitation of potential field method, which is a symmetrically aligned robot-obstacle-goal (SAROG) [43] as shown in Figure 6. APF method has a lower computational requirement than local planning approaches [40]. These forces are described as follow:

$$F_{att} = \alpha \left[(x_{target} - x_{uav})^2 + (y_{target} - y_{uav})^2 + (z_{target} - z_{uav})^2 \right], \tag{10}$$

$$F_{rep} = \frac{\varepsilon}{\sum_{t=1}^{m} \left[(x_{obstacle_t} - x_{uav})^2 + (y_{obstacle_t} - y_{uav})^2 + (z_{obstacle_t} - z_{uav})^2 \right]}. \tag{11}$$
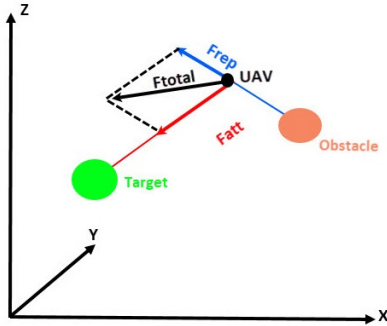
Figure 5. Normal situation of APF   **Figure 6.** Critical risk of local minima traps
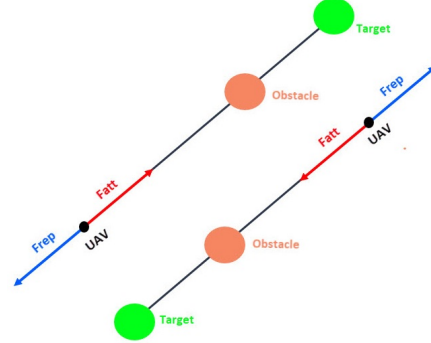
While the escape force was calculated based on the distances of the obstacle from the collision-free area as shown in Figure 7, we take into consideration the UAV's orientation in space:

$$F_{esc} = \begin{cases} 0, \text{ if No\_SARGO,} \\ 3D\_Cartesian\_Coordinate\_Rotation\_\left(\cos^{-1}\left(\frac{r_o + sd}{dv} \right) \right), \text{ if SARGO,} \end{cases} \tag{12}$$

$$\begin{bmatrix} x' \\ y' \\ z' \end{bmatrix} = BCD \begin{bmatrix} x \\ y \\ z \end{bmatrix}, \tag{13}$$

where the 3D Cartesian coordinate rotation is the BCD Euler's rotation matrices with $(-\pi < \theta < \pi)$ as follow:

$$D = \begin{bmatrix} \cos\varphi & \sin\varphi & 0 \\ -\sin\varphi & \cos\varphi & 0 \\ 0 & 0 & 1 \end{bmatrix}, \quad C = \begin{bmatrix} 1 & 0 & 0 \\ 0 & \cos\theta & \sin\theta \\ 0 & -\sin\theta & \cos\theta \end{bmatrix}, \quad A = \begin{bmatrix} \cos\psi & \sin\psi & 0 \\ -\sin\psi & \cos\psi & 0 \\ 0 & 0 & 1 \end{bmatrix}. \quad (14)$$

Figure 8 shows the axes' order around which to rotate the coordinates.

Also, $\begin{bmatrix} x \\ y \\ z \end{bmatrix}$, $\begin{bmatrix} x' \\ y' \\ z' \end{bmatrix}$ are the old and new coordinates of the UAV, respectively. This force applies when SARGO occurs; this is when the UAV, the obstacle, and the target are aligned or when the target and obstacle are closely positioned. This causes oscillation and is called local minima trap. The problem condition is described as:

$$\left[(x_2 - x_1)\hat{X} + (y_2 - y_1)\hat{Y} + (z_2 - z_1)\hat{Z}\right] \times \left[(x_3 - x_1)\hat{X} + (y_3 - y_1)\hat{Y} + (z_3 - z_1)\hat{Z}\right] \leq \vec{c}, \quad (15)$$

where, $\vec{c}$ is the vector that specifies the margin, where the UAV and target are located in regard to the obstacle.
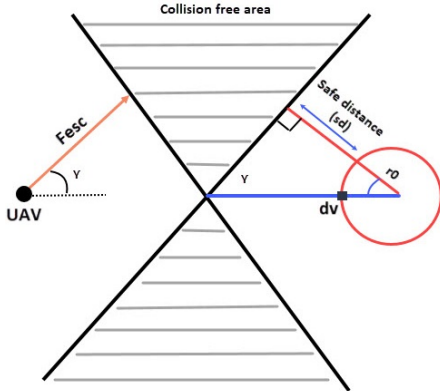
Figure 7. Escape force calculation method
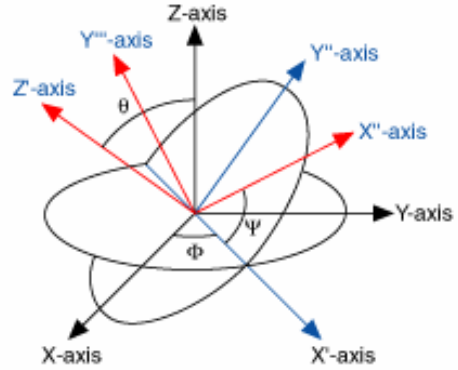
Figure 8. 3D Cartesian coordinate rotation based on Euler's rotation

GENETIC ALGORITHMS

Bio-inspired algorithms brought in heuristic ideas, and they can excellently deal with complex and dynamic unstructured constraints [3]. It is the most popular population-based optimization method. The basic version of GA defines a cost function to evaluate the potential solutions, which are the optimal waypoints on each k level along the path. This algorithm starts by selecting randomly feasible waypoints as the first generation. Then it takes the environment, dynamic ability, target, and other constraints into consideration, to evaluate the fitness of each individual (waypoint). In the next step, a set of individuals is selected as parents for the next generation according to their fitness. The last step is a mutation and crossover step. The whole process is performed in an iterative way and the process stops when a preset goal is achieved. The best fitness waypoints are marked as the optimal path nodes achieved the shortest path to target and far away from the obstacle for each segment k as follows:

$$J_k = hJ_{ek} + (1-h)J_{ok} = h\sum_{i=1}^{n} D_{eik}{}^2 + (1-h)\sum_{t=1}^{m}\sum_{i=0}^{n} \frac{1}{D_{o_{t,ik}}{}^2}. \tag{16}$$

There are five parameters in GA algorithms, namely maximum generation number, length of solution (number of waypoints in this case study), population size, mutation, and crossover. Generally, solutions can evolve further when generation number is increased. The length of solution decides the complexity of the problem while population size, mutation, and crossover alter the performance of GA.

SIMULATION

Processes of testing and simulation were made using LabView software. In first simulation process of APF algorithm we suppose simple scenario as shown in Figure 9, where start point is (0, 0, 0), target point is (0, 15, 40), orange spheres are randomly generated obstacles which parameters are presented in Figure 10. This algorithm is characterized by the ability to work in real time without the need for preprocessing of the map in comparison with other algorithms. However, it requires precise adjustment and adaptation of the parameters of attraction, repelling, and escape $\alpha = 1E^{-6}$, $\varepsilon = 0.8$, $sd = 0.3$, $dv = 4r_o$, in order to get a better and more realistic path. The algorithm suffers from the trap problem that was explained before, when the aircraft is in the same plane with the target and the obstacle and was solved by the escape force. This solution is considered insufficient and requires testing and evaluation to define the extent of effectiveness.
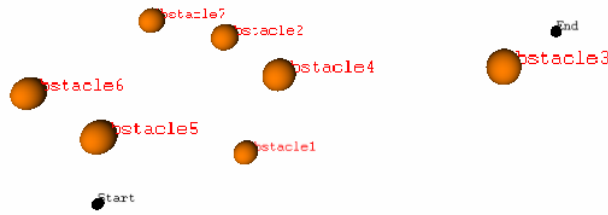
Figure 9. The scenario of testing the APF algorithm in a 3D environment

Figure 10. A diagram illustrating the location and the number of the spherical shapes

Simulation depends on assuming that the aircraft is a point in space regardless of motion constraints represented by motion. That is why the algorithm requires some modifications of adding flying constraints and adding adaptive techniques for automatic modification of the algorithm parameters in order to get quicker decision when overtaking obstacles of constant radius, presumably for all the obstacles, including the value of the distance between the obstacles and the target and between them and the vehicle; also, the SARGO distance that is defined according to the trap condition equation; additionally, indicators that define the trap state and a state that defines overtaking the obstacle. The obtained results of this test are due to pure mathematical operations represented by applying the mathematical vectors techniques in executing the algorithm according to [17–18] as shown in Figure 11. However, with a 3D generalization to find a solution for a multi-target problem represented by keeping away from obstacles and getting near from the target. The vector applied on the vehicle is unfeasible; there are no constraints on it. Implementing a planner for the motion path of an unmanned aerial vehicle requires making modification by imposing constraints on the motion vector along with scaling to transform the vector from pure mathematical to realistic vector. The following figures show the vector values.
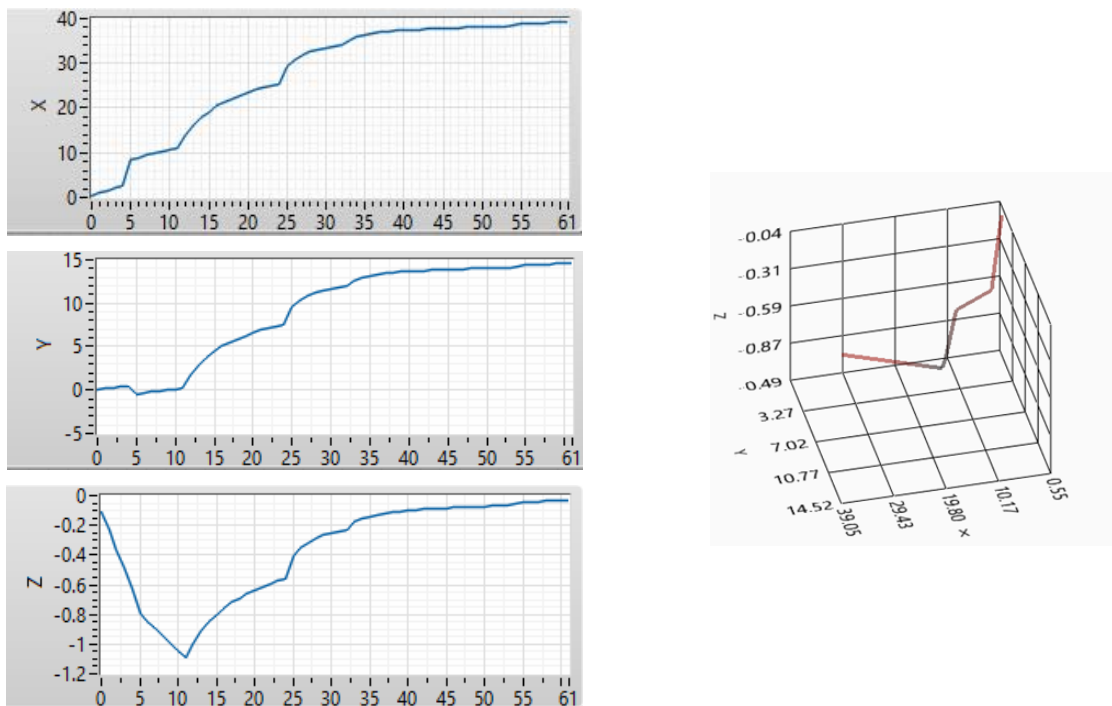
Figure 11. The results of applying APF method and coordinate vectors in 3D view

In the second simulation the GA algorithm was applied as a suggestion of a navigation algorithm with several testing scenarios, which is characterized by being more complex and contains 60 spherical obstacles of fixed diameters, generated randomly. These scenarios require making some prior transformations and maintaining a suitable height. This is to simplify the calculations as mentioned before. This theory does not work instantaneously, requires iterative processing, and consumes processing time. In real world, the shapes of obstacles are not spherical as proposed in previous scenarios. In order to apply the algorithms, it is necessary to make an approximation, which converts the obstacle into a spherical form. The following figures from 12 to 15 illustrates the phases of checking the algorithm with modifying the algorithm parameters in addition to comparing the results.
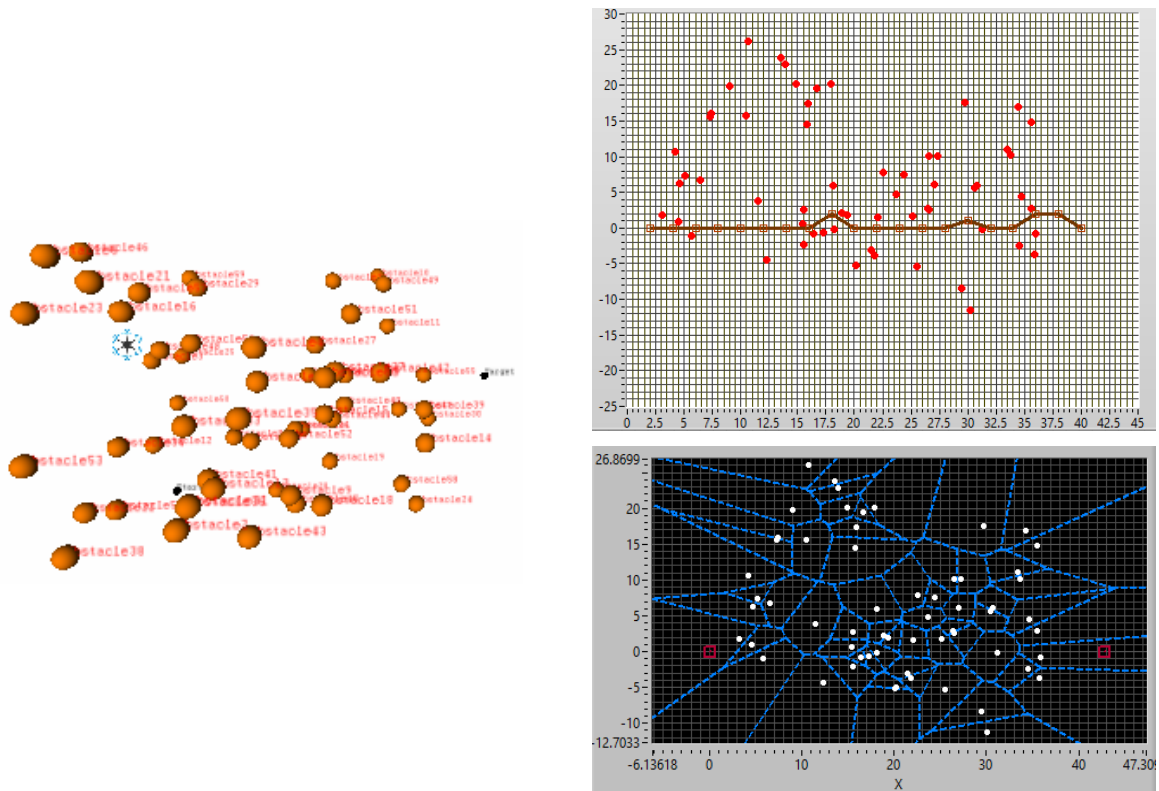
Figure 12. The results of applying the genetic algorithm in 3D environment with 60 obstacles and by using following parameters: segment length ST = 2, population size = 12, generation iterations = 12, crossover parameter = 0.9, mutation parameter = 0.03
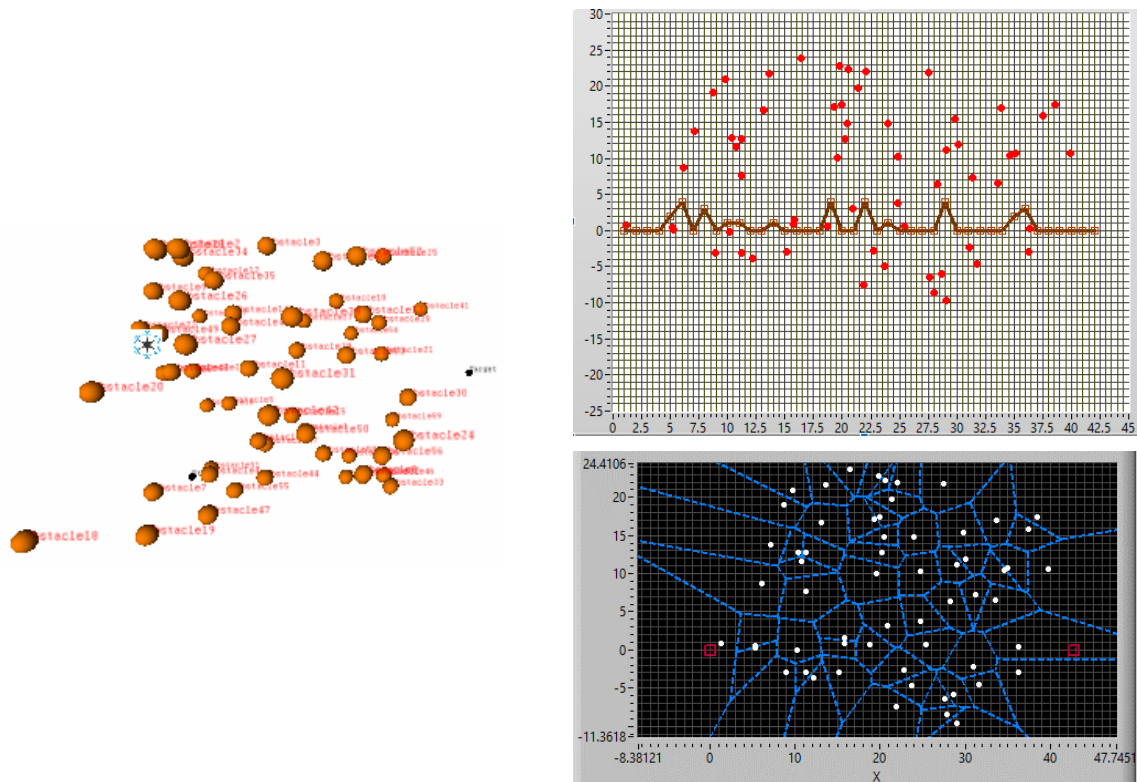
Figure 13. The results of applying the genetic algorithm in 3D environment with 60 obstacles and by using following parameters: segment length ST = 1, population size = 12, generation iterations = 12, crossover parameter = 0.9, mutation parameter = 0.03
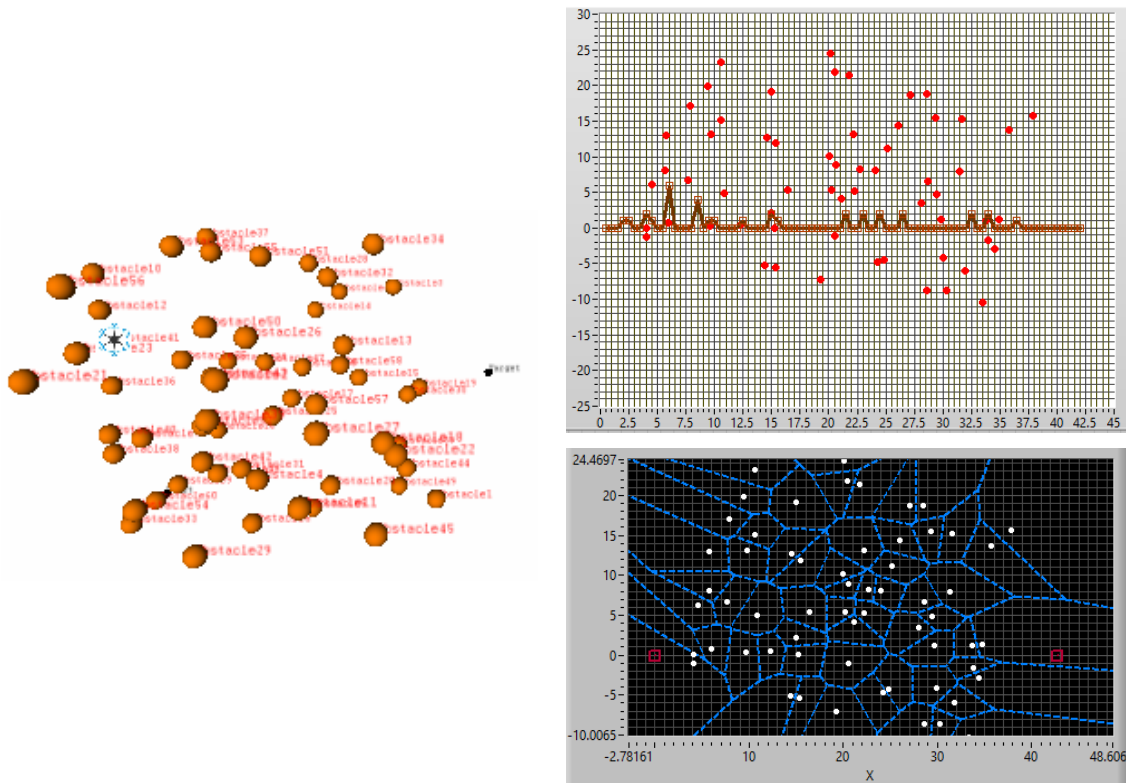
Figure 14. The results of applying the genetic algorithm in 3D environment with 60 obstacles and by using following parameters: segment length ST = 0.5, population size = 12, generation iterations = 12, crossover parameter = 0.9, mutation parameter = 0.03
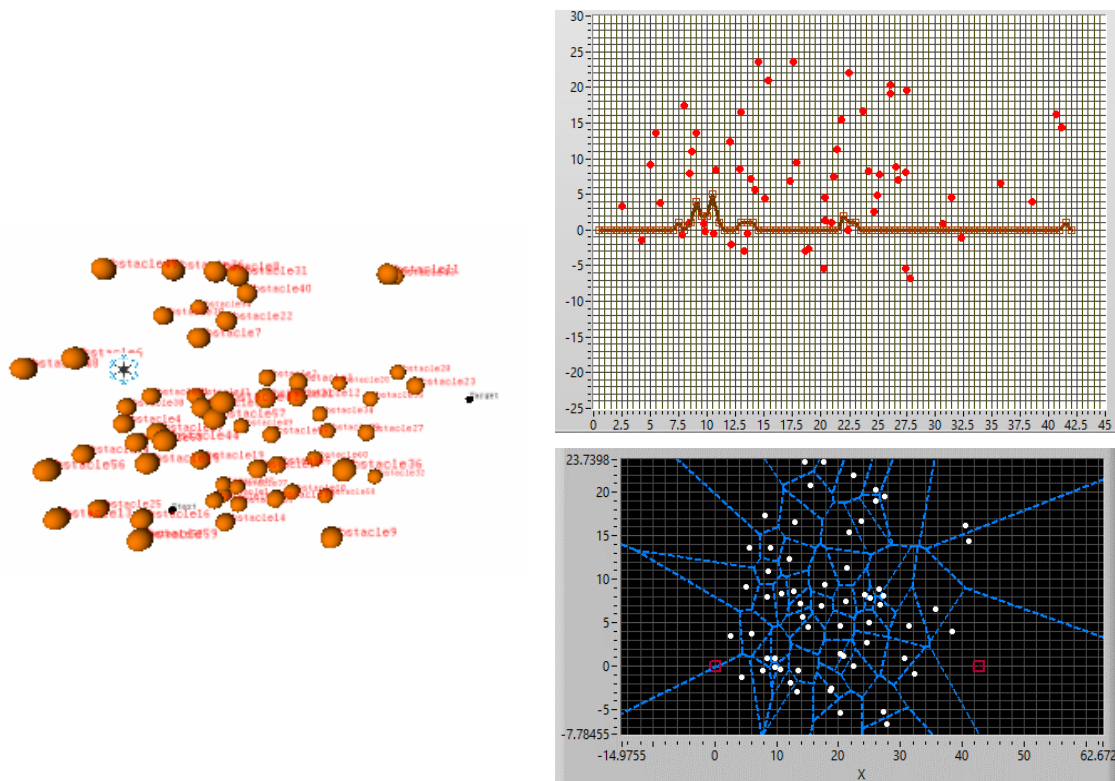
Figure 15. The results of applying the genetic algorithm in 3D environment with 60 obstacles and by using following parameters: segment length ST = 0.5, population size = 20, generation iterations = 20, crossover parameter = 0.9, mutation parameter = 0.03

Conclusion

This paper offers a comparison between two procedures of 3D navigation to prevent collision of an unmanned vehicle in space. The effectiveness of the two algorithms are defined according to computer simulation, and mathematically it is possible to modify the APF algorithm in order to get improvements in the path by adding constraints on motion and adjusting the parameters continually in order to get path planning that works in a real time. On the other hand, the genetic algorithm is considered ideal; it works in complex dynamic environments and does not require prior information about the search field. Due to the experiments, it also requires the precise adjustment of the parameters in order to get an ideal path, but it consumes processing time because its work is iterative. For applying both algorithms in flying, more detailed investigation is required. The following table 1 shows time complexity, work stages, and the environments as a comparison between the two algorithms.

Table 1. Time complexity and the environments as a comparison between the two algorithms

Method	Time Complexity	S/D Environment	Real-Time
APF Sampling-based Algorithm	$O\left(n\log(n)\right) \leq T \leq O\left(n^2\right)$	Static and Dynamic obstacles	On-line
GA Bio-inspired Algorithm	$T \geq O\left(n^2\right)$	Static and Dynamic obstacles	Off-line

References

1. Tsai, Y. J., Lee, C. S., Lin, C. L., & Huang, C. H. (2015). Development of flight path planning for multirotor aerial vehicles. *Aerospace, 2*(2), 171–188. doi:10.3390/aerospace2020171.

2. Bagherian, M., & Alos, A. (2015). 3D UAV trajectory planning using evolutionary algorithms: a comparison study. *The Aeronautical Journal, 119*(1220), 1271–1285. doi:10.1017/S0001924000011246.

3. Yang, L., Qi, J., Song, D., Xiao, J., Han, J., & Xia, Y. (2016). Survey of robot 3D path planning algorithms. Journal of Control Science and Engineering, 2016, article ID 7426913, 22 pp. doi:10.1155/2016/7426913.

4. Gouda, B. K. (2006). Optimal robot trajectory planning using evolutionary algorithms (Masters thesis, Cleveland State University, USA). Retrieved from: https://academic.csuohio.edu/embedded/Publications/Thesis/Gouda Thesis.pdf.

5. Zhang, L., Liu, Z., Papavassiliou, C., & Liu, S. (2017). Formation path control method for group coordination based on fuzzy logic control method. *Cluster Computing,* 1–14. doi:10.1007/s10586-017-0924-2.

6. Adhikari, D., Kim, E., & Reza, H. (2017, June). A fuzzy adaptive differential evolution for multi-objective 3D UAV path optimization. In *Evolutionary Computation (CEC), 2017 IEEE Congress on (pp. 2258–2265).* doi:10.1109/CEC.2017.7969578.

7. Kok, K. Y., & Rajendran, P. (2016). Differential-evolution control parameter optimization for unmanned aerial vehicle path planning. *PLoS ONE, 11*(3), e0150558. doi:10.1371/journal.pone.0150558.

8. Zhu, W., & Duan, H. (2014). Chaotic predator–prey biogeography-based optimization approach for UCAV path planning. *Aerospace science and technology, 32*(1), 153–161. doi:10.1016/j.ast.2013.11.003.

9. Xu, C., Duan, H., & Liu, F. (2010). Chaotic artificial bee colony approach to Uninhabited Combat Air Vehicle (UCAV) path planning. *Aerospace Science and Technology, 14*(8), 535–541. doi:10.1016/j.ast.2010.04.008.

10. Wang, Q., & Zhang, J. (2017, July). MPC and TGFC for UAV real-time route planning. In *Control Conference (CCC), 2017 36th Chinese* (pp. 6847–6850). Dalian, China: IEEE. doi:10.23919/ChiCC.2017.8028436.

11. Shen, H., Chen, J., Li, H., & Zhou, Z. (2016, December). Research on real-time flight path planning of UAV based on grey prediction. In *2016 9th International Symposium on Computational Intelligence and Design (ISCID)* (Vol. 1, pp. 62–67). Hangzhou, China: IEEE. doi:10.1109/ISCID.2016.1023.

12. Kurnaz, S., Cetin, O., & Kaynak, O. (2009). Fuzzy logic based approach to design of flight control and navigation tasks for autonomous unmanned aerial vehicles. *Journal of Intelligent and Robotic Systems, 54*(1–3), 229–244. doi:10.1007/s10846-008-9263-0.

13. Kurnaz, S., Cetin, O., & Kaynak, O. (2010). Adaptive neuro-fuzzy inference system based autonomous flight control of unmanned air vehicles. *Expert Systems with Applications, 37*(2), 1229–1234. doi:10.1016/j.eswa.2009.06.009.

14. Vadakkepat, P., Tan, K. C., & Ming-Liang, W. (2000). Evolutionary artificial potential fields and their application in real time robot path planning. In *Proceedings of the 2000 Congress on Evolutionary Computation, 2000* (Vol. 1, pp. 256–263). La Jolla, CA, USA: IEEE. doi:10.1109/CEC.2000.870304.

15. Khatib, O. (1986). Real-time obstacle avoidance for manipulators and mobile robots. *The International Journal of Robotics Research, 5*(1), 90–98. doi:10.1177/027836498600500106.

16. Hoy, M., Matveev, A. S., & Savkin, A. V. (2015). Algorithms for collision-free navigation of mobile robots in complex cluttered environments: a survey. *Robotica, 33*(3), 463–497. doi:10.1017/S0263574714000289.

17. Wang, C., Savkin, A. V., & Garratt, M. (2016). Collision free navigation of flying robots among moving obstacles. In *2016 35th Chinese Control Conference (CCC)* (pp. 4545–4549). Chengdu, China: IEEE. doi:10.1109/ChiCC.2016.7554058.

18. Lee, J., Nam, Y., & Hong, S. (2010). Random force based algorithm for local minima escape of potential field method. In *2010 11th International Conference on Control Automation Robotics & Vision (ICARCV)* (pp. 827–832). Singapore, Singapore: IEEE. doi:10.1109/ICARCV.2010.5707422.

19. Shamos, M. I., & Hoey, D. (1975). Closest-point problems. In *Proceedings of the 16th Annual Symposium on Foundations of Computer Science* (pp. 151–162). Berkeley, Calif, USA: IEEE. doi:10.1109/SFCS.1975.8.

20. Luchnikov, V. A., Medvedev, N. N., Oger, L., & Troadec, J.-P. (1999). Voronoi-Delaunay analysis of voids in systems of nonspherical particles. *Physical review E, 59*(6), 7205–7212. doi:10.1103/PhysRevE.59.7205.

21. Ibrahim, I. N., Pavol, B., Al Akkad, M. A., & Karam, A. (2017). Navigation control and stability investigation of a hexacopter equipped with an aerial manipulater. In *2017 21st International Conference on Process Control (PC)* (pp. 204–209). Strbske Pleso, Slovakia: IEEE. doi:10.1109/PC.2017.7976214.

22. Ibrahim, I. N., Al Akkad, M. A., & Abramov, I. V. (2017). Attitude and altitude stabilization of a microcopter equipped with a robotic arm. In *2017 International Siberian Conference on Control and Communications (SIBCON)* (pp. 1–8). Astana, Kazakhstan: IEEE. doi:10.1109/SIBCON.2017.7998561.

23. Ibrahim, I. N., Hussin, S., & Abramov, I. V. (2017). Minicopter nonlinear control with the existence of disturbances. In *Instrumentation Engineering, Electronics and Telecommunications – 2016: Proceedings of the International Forum* (pp. 21–33). Izhevsk, Russia: Kalashnikov Izhevsk State Technical University. ISBN: 978-5-7526-0767-7.

24. Ibrahim, I. N., & Al Akkad, M. A. (2017). Studying the disturbances of robotic arm movement in space using the compound-pendulum method. *Bulletin of Kalashnikov ISTU, 20*(2), 156–159. doi:10.22213/2413-1172-2017-2-156-159.

25. Ibrahim, I. N., Al Akkad, M. A., & Sosnovich, E. V. (2017). Optimization of hexacopter stability control with disturbances in its stochastic state space dynamics model. *55th International Scientific Conference on Experimental Stress Analysis 2017 (EAN 2017): Conference Proceedings* (pp. 731–739). Novy Smokovec, Slovakia: Technical University of Kosice. ISBN: 978-805533167-6.

Feature Extraction Model
in Systems of Diagnostics of Plant Diseases by the Leaf Images

N. Mirzaev [1], E. Saliev [2]

Scientific-Innovation Centre of Information-Communication Technologies at the
Tashkent University of Information Technologies Named after Muhammad al-Khorezmi,
Tashkent, Republic of Uzbekistan
E-mail: [1] nomazmirza@rambler.ru, [2] salievea@gmail.com

Abstract. The task of features extraction occurring in creation of systems to diagnose crop diseases using leaves images has been examined in this work. The model of diagnostic feature extraction of leaves images has been proposed for the problem solution. The main concept of the proposed model includes creation of preferred feature set simplifying the construction process of considered rule in pattern recognition given in the form of images. Experimental investigations at problem solving on diagnosis of wheat diseases with the help of leaves images have been conducted for function test of the presented model.

Keywords: diagnostic systems, base fragments of images, diagnostics of plant diseases, diagnostic features of leaves, preferred features, correlation of features.

INTRODUCTION

The issues of creation and use of information systems and technology in agricultural production under modern conditions become a key factor of innovation activities and scientific and technological progress in the field [1]. One of the major tasks in the sphere of modern IT application has to do with the creation of computer systems for identification of crop diseases and forecasting of their development.

It is known that measurement technique is a key factor of scientific and technology development in all sectors of the national economy. Nowadays, information-measuring systems (IMS) are broadly used among the various types of measuring tools due to the requirements of production, trade and other spheres of human activity. Moreover, the scope of IMS use grows continuously.

Over the last years the number of published works have been increased in the field of information systems creation, especially IMS almost in every direction of the agricultural science and production [1-14]. This fact is connected with information and analysis support of experts' intellectual activity that provides productivity in the subject area of industrial technology.

Today qualifying operations have become an integral part of manufacturing processes. The issues of creation and use of IMS in agricultural production under the modern conditions become a key factor of innovation activities in the field.

One of the main tasks in the scope of application of modern IMS has to do with the creation of information systems for identification of crop diseases, forecasting of their development and spread of crop pests. It is related to the fact that the problem of plant protection from harmful organisms is the most significant which involves the interests of the State [14]. In addition to this, it is evident that without unbiased information on pest condition, diseases and crop weeds, on the one hand, and environment and its trend change on the other hand, practical implementation of protective measures is connected with high expenditures. The application of information system of diagnostics and control phytosanitary condition allows improving reliability of information with the help of diagnostics that gives an opportunity for implementation of earlier and more accurate crop disease diagnosis and make decisions on taking measures to protect them [7–9]. In connection to this, creation of information systems of blights diagnostics (including wheat) is a vital task in controlling of crop harvest. This fact lays the groundwork for frequent occurrence of scientific researches where the issues on blight diagnosis are considered [3, 6–9, 12]. For example, the problems of crop diseases diagnostics have been examined in this work [12] using artificial neural networks. The fundamental idea of the study is a separation of color and textural features of the leaves images. The problems of information system creation of hips diseases of crop have been studied in the work [11] on the basis of image processing of their leaves. The issues of leaves images processing have been analyzed in the paper [13].

The source literature analysis, in particular [2–14], shows that the problem of crop disease diagnosis has not been enough studied. Therefore, the objectives associated with the questions of information extraction on the examined plants given in the form of leaves images are still important today.

The distinctive feature of the studied approach to the problem solution of features selection is the set formation of preferential characteristics simplifying the construction of decision procedure in the object recognition set in the form of pictures. Moreover, it helps to accomplish transition from specific algorithms of feature selection to the model – a family of algorithms for uniform description of the decision procedure. It should be noted that the present paperwork represents an updated and revised version [14].

The aim of the study is the development of formation model of diagnostic features defining crop disease by source picture of leaves. The approach which is used here is based on the statistical analysis of leaves pictures of the diagnosed crops.

In order to gain the above set goal it is necessary to solve the following tasks:

1) to make reappraisal of the existed approaches to problem solving of crop diseases by the leaves photos and define the research objectives;

2) to develop a model of the image feature extraction associated with identification of crop blights by the leaves pictures;

3) to carry out experimental research for performance evaluation of the developed model.

From a scientific perspective the findings of the work represent a new solution to the scientific learning connected with the object recognition submitted in a form of images. The practical significance of the obtained results is that the engineered algorithms and programs can be used in solving of applications in relation to the object identification presented in the form of images (for instance, in the problems of crop diseases diagnosis with the help of leaves pictures, person identification by a portrait).

STATEMENT OF THE PROBLEM

We consider the set of admissible objects $\mathfrak{M}$, given as images of plants leaves. Initial data on each admissible object (investigated plant) $\mathfrak{I}$ are given three dimensional matrix

(color image) X with the size $c \times m \times n$ (where c – the number of color channels; m and n – the numbers of rows and columns respectively):

$$X = \begin{vmatrix} x_{c11} & \ldots & x_{ci1} & \ldots & x_{cn1} \\ \ldots & \ldots & \ldots & \ldots & \ldots \\ x_{c1j} & \ldots & x_{cij} & \ldots & x_{cnj} \\ \ldots & \ldots & \ldots & \ldots & \ldots \\ x_{c1m} & \ldots & x_{cim} & \ldots & x_{cnm} \end{vmatrix}. \tag{1}$$

It is assumed that the objects of the set $\Re$ are divided into two disjoint subsets (of the class) K_1 and K_2 [15]:

$$\Re = \bigcup_{j=1}^{2} K_j, \quad K_1 \cap K_2 = \varnothing. \tag{2}$$

The division $\Re$ is not completely defined. There is only some initial information J_0 about the classes K_1, K_2. Let there be some sample $\tilde{\Im}^m$ ($\tilde{\Im}^m \subset \Re$) consisting of m objects ($\tilde{\Im}^m = \{\Im_1, ..., \Im_i, ..., \Im_m\}$, $\Im_i \in \Re$, $i = \overline{1, m}$):

$$\tilde{K}_j = \tilde{\Im}^m \cap K_j, \quad C\tilde{K}_j = \tilde{\Im}^m \setminus \tilde{K}_j. \tag{3}$$

Then the initial information J_0 about the classes can be given in the form [15]:

$$J_0 = \{\Im_1, \tilde{\alpha}(\Im_1); ...; \Im_i, \tilde{\alpha}(\Im_i); ...; \Im_m, \tilde{\alpha}(\Im_m)\}, \quad \tilde{\alpha}(\Im_i) = (\alpha_{i1}, \alpha_{i2}), \tag{4}$$

where α_{ij} – value of the predicate $P_j(\Im_i) = "\Im_i \in K_j"$.

The task is to build such an operator that allows to form a space of features that characterizes the diseases of cultivated plants according to the initial image of the leaves. The determination of the set of diagnostic features $\{\tau_{u1}, ..., \tau_{ui}, ..., \tau_{un}\}$ is carried out according to the given initial information J_0 on the basis of statistical analysis. In this case, it is required that the formed feature space be smaller than the original one, and it should ensure the separation of the specified objects with some accuracy.

PROPOSED APPROACH

A non-standard approach to the problem of feature set formation identifying crop diseases has been studied in the research. The model of feature extraction of the object set in the form of images has been offered on the basis of this approach. A fundamental concept of the proposed model involves space creation of independent (or weakly dependent) diagnostic features in pattern recognition given in the form of images. Therewith three-dimensional (two-dimensional) structure of leaves images is introduced as one-dimensional space of characteristics of high dimensionality. Each feature defines only a specific area (fragment) of a picture. Various statistical characteristics are used for description of each fragment of an initial picture.

The proposed model of operators for extracting the diagnostic features of images of leaves of cultivated plants includes the following main steps.

1. Formation of basic fragments of images of leaves. The first step in setting the model for the extracting of features is the formation of a system of basic fragments of images Σ, where $\Sigma = \{\Xi_1, ..., \Xi_k\}$, depending on the parameter k, where $k = m_H \times n_W$, m_H is the number

of vertical divisions of the image, and n_W is the number of image divisions by width. This parameter indicates the fixed power of the subsets that are formed as a result of the division of the image in question. By specifying different integer values for this parameter, different amounts of base fragments can be obtained. This requires that the number of elements (pixels) in each image fragment should be the same. As a result of this stage, k the same rectangular fragments are formed. If the dimension of the original image is $H \times W$ pixels, then the resulting image fragments will consist of $k_H \times k_W$ pixels:

$$k_H = H \operatorname{div} m_H + \delta_H, \qquad k_W = W \operatorname{div} n_W + \delta_W,$$
$$\delta_H = \begin{cases} 0, & \text{if } H \bmod m_H = 0, \\ 1, & \text{else;} \end{cases} \qquad \delta_W = \begin{cases} 0, & \text{if } W \bmod n_W = 0, \\ 1, & \text{else.} \end{cases} \tag{5}$$

If there are residuals from division, the sizes of image fragments are increased by one pixel, the beginning of the others is shifted to the left (up) by one pixel.

Depending on the method of forming the system of basic fragments Ξ_q, where $q = \overline{1,k}$, we can get a variety of feature extraction algorithms [16].

2. Determining of a set of diagnostic features of leaves. At this stage, a set of diagnostic features is formed, which are defined as sampling points on the reference subset in question. It is known [17] that the moment of order n_p, where $n_p = (p+q)$, of the random variable $f(x,y)$, where $(x,y) \in \Xi_u$, is defined as

$$m_{pq} = \frac{1}{N_u} \sum_{(x,y) \in \Xi_u} x^p y^q f(x,y), \quad N_u = |\Xi_u|, \quad p,q = 0,1,...,n_P, \tag{6}$$

here n_P is a parameter indicating the maximum order of the computed moments.

To determine the central moments, we use the following formula:

$$\mu_{pq} = \frac{1}{N_u} \sum_{(x,y) \in \Xi_u} \left(x - \overline{x}_u\right)^p \left(y - \overline{y}_u\right)^q f(x,y), \tag{7}$$

where $\overline{x}_u$ and $\overline{y}_u$ coordinates of the central point Ξ_u.

In addition to the characteristics considered, it is possible to calculate variance, autocorrelation, etc., as diagnostic features of the object.

As a result of this stage, we get a set of diagnostic features. The generated feature space will be denoted by Υ ($\Upsilon = (y_1,...,y_{k \times n_P})$).

3. Extracting of subsets of strongly correlated features. At this stage, a system of "independent" subsets of diagnostic features Υ is defined.

The subsets of strongly correlated features are extracted as follows. Let $\Gamma_u(u = \overline{1,k'})$ - be subsets of diagnostic strongly correlated features. The proximity measure $L(\Gamma_u, \Gamma_v)$ between the subsets Γ_u and Γ_v may be given with different ways, for example:

$$L(\Gamma_u, \Gamma_v) = \frac{1}{N_u \cdot N_v} \sum_{y_i \in \Gamma_u} \sum_{y_j \in \Gamma_v} \eta(y_i, y_j), \tag{8}$$

where N_u, N_v − the number of diagnostic features entering respectively into subsets Γ_u and Γ_v; $\eta(y_i, y_j)$ − function characterizing the strength of the pair relationship between the signs y_i and y_j.

As a result of this stage, a set of "independent" subsets of strongly correlated features $W_A = \{\Xi_1, \Xi_2, ..., \Xi_{n'}\}$ is determined. The number of extracted subsets will depend on the parameter n'. By setting this parameter to various integer values, we can get different algorithms [18].

4. Determining of preferred features. We consider the subsets $\{\Xi_1, ..., \Xi_q, ..., \Xi_{n'}\}$, which are defined in the previous step. Let N_q be the power of a subset of strongly correlated features. A selection from a subset Ξ_q the preferred feature is made on the basis of an evaluation of the dominance of the feature in question, which divides the objects belonging to the set $\tilde{\mathfrak{I}}^m$ into two subsets (classes) K_1 and K_2 [19]:

$$D_i = \frac{\hat{N}_2 \sum_{j=1}^{2} \sum_{\mathfrak{I} \in \tilde{K}_j} \sum_{\mathfrak{I}_u \in \tilde{K}_j} (a_i - a_{iu})^2}{\hat{N}_1 \sum_{\mathfrak{I} \in \tilde{K}_1} \sum_{\mathfrak{I}_u \in \tilde{K}_2} (a_i - a_{iu})^2}, \tag{9}$$

where $\hat{N}_1 = \left(m_1(m_1 - 1) + m_2(m_2 - 1) \right)/2$, $\hat{N}_2 = m_1 \times m_2$, $m_1 = \left| \tilde{K}_1 \right|$, $m_2 = \left| \tilde{K}_2 \right|$.

The smaller the value D_i, the greater the preference is given to the corresponding feature. If two or more features receive the same preference, then any one of them is selected. In calculating D_i, it is assumed that $\mathfrak{I}$ and $\mathfrak{I}_u$ are different objects (i.e. $\mathfrak{I} \neq \mathfrak{I}_u$).

For each subset of strongly correlated features Ξ_q, a preferred feature is identified at this stage, which is denoted by χ_q. As a result, the following set of preferred features is formed: $\chi_1, \chi_2, ..., \chi_{n'}$.

Each preferred feature from this set is representative of only one subset of strongly correlated features.

Thus, a model of operators for the formation of diagnostic features for the image of leaves of cultivated plants is defined. To assess the efficiency of the model, experimental studies were conducted.

In order to assess the working capacity of the model, functional schemes and corresponding algorithms have been developed that determine the structure of the program to be created.

EXPERIMENT AND RESULTS

Functional diagrams and relevant diagnosis programs have been developed for common use and performance evaluation of the analysed model. The elaborated programs have been implemented in Delphi language. For the purposes of functional test of the developed programs we shall consider the diagnosis task of the stripe rust of wheat using leaves images.

The fact is that rust diseases of grain, especially wheat, are more harmful and dangerous in many parts of the world. The injuriousness of these wheat diseases and volumes of harvest losses depend on a number of factors, primary lesion period (i.e. phases of wheat growth, starting time of a disease), growth rate and others.

A precise determination of phase of development is of great importance not only in the analysis of harmful rust diseases but also in the conducting of research on forecasting of disease development and plan organization for plant protection.

A precise determination of phase of development is of great importance not only in the analysis of harmful rust diseases but also in the conducting of research on forecasting of disease development and plan organization for plant protection.

The collection of 300 wheat leaves images is given as initial data (i.e. original sample V). Furthermore, a number of possible diagnoses (phytosanitary state) equals 2:

- wheat leaves images with detected stripe rust (K_1);

- wheat leaves images without stripe rust (K_2).

The first subset K_1 has 150 pictures and the second – the rest. These pictures have been divided into educational and check samples. The method of cross-validation is applied for accuracy calculation at problem solving for the exception purposes of successful (or unsuccessful) partition of the original sample V into two parts V_o and V_k ($V = V_o \cup V_k$, where V_o – training set, V_k – test set) [18, 20]. In this technique the original sample of objects is split into 30 non-crossing blocks in a random manner containing 10 objects each. It is required to keep proportion in all blocks quantitatively to objects belonging to different classes. As the result 5 objects of each class can be observed in each block. The procedure of cross-validation in these blocks includes several steps. 22 from 30 blocks are chosen on each step in the function of educational sample, and the model with set parameters is taught at this sampling. The model taught in such a way is checked in other 8 blocks (check sample). The model quality rating on accuracy classification is identified and recorded at the end of each control. Each block one by one is selected and their positions are changed when implementing every next step from test and training sets. The appropriate blocks are marked and they do not participate when selecting candidates for including control sample to exclude objects reuse of check samples. The correctness of diagnosis is defined as average after finishing the procedure of cross-validation exam.

The task of diagnostics has been completed with the help of: 1) the model described in [11]; 2) the proposed model of feature extraction. Experimental results in problem solving with the use of these models are presented, correspondingly, in the Tables 1 and 2.

Table 1. The results of solving the diagnostic problem using the known model

Diagnosis	The average number of correct diagnoses	The average number of incorrect diagnoses	Average number of failures	Accuracy of diagnosis
Sick	32.1	6.4	1.5	80.3 %
Not sick	34.6	4.5	0.9	86.5 %

Table 2. The results of solving the diagnostic problem using the developed model

Diagnosis	The average number of correct diagnoses	The average number of incorrect diagnoses	Average number of failures	Accuracy of diagnosis
Sick	36.3	2.9	0.8	90.8 %
Not sick	37.6	1.9	0.5	94.0 %

According to Table 1, when using the model considered in [11], 66.7 objects from 80 objects (images of leaves) were properly identified on average, which is 83.4% recognition accuracy. Using the developed model, 73.9 objects were correctly identified from 80 objects (images of leaves), which is 92.4% recognition accuracy (Table 2).

The carried out experimental researches have shown the efficiency of the developed model of extraction of diagnostic features in solving the given task. As a result of the experiment, a set of diagnostic features is generated, which allows to split the objects of the control sample into two classes with an acceptable error.

CONCLUSION

The issues on diagnostics of crop diseases and data support of decision-making on their protection are one of the main in the problem of harvest control. Nevertheless, tasks connected with the development of automated systems of crop diseases diagnostics are not studied well.

The model of diagnostic feature creation has been developed in the detection of blights using leaves images. Moreover, formation of diagnostic features is supported by calculation of different statistical characteristics for each fragment of the initial picture.

In the course of solving a practical task it has been specified that the steps of subset formation of "independent" features, especially, issues on detection of a number of such subsets and collection of diagnostic features by leaves pictures as well as extraction of preferable characteristics play the most important role in task solving of diagnostics. Therefore, it is necessary to continue research taking into account the ascertained directions.

The developed model can be employed in composition of diverse software applications focused on decision-making of objects classification prescribed in the form of images.

REFERENCES

1. Alt, V. V. (2006). Informatsionnyye tekhnologii kak faktor povysheniya effektivnosti vybora tekhnologicheskikh resheniy [Information technologies as a factor in increasing the efficiency of the choice of technological solutions]. *Dostizheniya nauki i tekhniki APK [Achievements of Science and Technology of AIC], 2006*(11), 3–5 (in Russian). Available at: https://elibrary.ru/item.asp?id=10333014.

2. Li, K., Xiong, L., Zhang, D., Liang, Z., & Xue, Y. (2017). The research of disease spots extraction based on evolutionary algorithm. *Journal of Optimization, 2017,* article ID 4093973, 1–14. doi:10.1155/2017/4093973.

3. Kadakol, S., & Maned, J. (2016). Intelligence system for leaf extraction and disease diagnostic. *International Journal of Computer Sciences & Engineering Engineering, 4*(3), 62–66. Retrieved from: http://www.ijcseonline.org/pdf_spl_paper_view.php?paper_id=64&14-I009-IJCSE.pdf.

4. Kaur, L., & Laxmi, V. (2016). A review on plant leaf classification and segmentation. *International Journal of Engineering and Computer Science, 5*(8), 17658–17661.

5. Shripriya, R., & Yuvaraj, N. (2016). A survey on leaf disease prediction algorithms using digital image processing. *Indian Journal of Innovations and Developments, 5*(10), 1–4. Retrieved from: http://ijid. informaticspublishing.com/index.php/ijid/article/view/111065.

6. Patil, R., Udgave, S., More, S., Nemishte, D., & Kasture, M. (2016). Grape leaf disease detection using k-means clustering algorithm. *International Research Journal of Engineering and Technology, 3*(4), 2330–2333.

7. Dange, D. J., & Sayyad, M. A. (2015). Computer vision image enhancement and plant leaves disease detection. *International Journal of Modern Trends in Engineering and Research, 2*(6), 106–110. Retrieved from: https://www.ijmter.com/papers/volume-2/issue-6/computer-vision-image-enhancement-and-plant-leaves-disease-detection.pdf.

8. Petrellis, N. (2015). Plant disease diagnosis based on image processing, appropriate for mobile phone implementation. In *Proceedings of the 7th International Conference on Information and Communication Technologies in Agriculture, Food and Environment (HAICTA 2015)* (pp. 238–246). Kavala, Greece. Retrieved from: http://ceur-ws.org/Vol-1498/HAICTA_2015_paper28.pdf.

9. Arivazhagan, S., Newlin Shebiah, R., Ananthi, S., & Vishnu Varthini, S. (2013). Detection of unhealthy region of plant leaves and classification of plant leaf diseases using texture features. *Agricultural Engineering International: CIGR Journal, 15*(1), 211–217. Retrieved from: http://www.cigrjournal.org/index.php/Ejounral/article/view/2338/1720.

10. Mondal, K. K., & Shanmugam, V. (2013). Advancements in the diagnosis of bacterial plant pathogens: An overview. *Biotechnology and Molecular Biology Review, 8*(1), 1–11. doi:10.5897/BMBR12.007.

11. Anami, B. S., Pujari, J. D., & Yakkundimath, R. (2011). Identification and classification of normal and affected agriculture/horticulture produce based on combined color and texture feature extraction. *International Journal of Computer Applications in Engineering Sciences, 1*(3), 356–360.

12. El-Helly, M., Rafea, A., & El-Gammal, S. (2003). An integrated image processing system for leaf disease detection and diagnosis. In *Proceedings of the 1st Indian International Conference on Artificial Intelligence (IICAI 2003)* (pp. 1182–1195). Hyderabad, India.

13. Denisyuk, V. S. (2008). Algoritmy vydeleniya osobennostey na izobrazheniyakh s tsel'yu klassifikatsii zabolevaniy rasteniy [Algorithms of image analysis for feature detection problem in order to diagnose plants diseases] (in Russian). In V. N. Kasyanov (Ed.), *Konstruirovaniye i optimizatsiya parallel'nykh programm [Parallel programs construction and optimization]* (pp. 71–82). Novosibirsk, Russia: A. P. Ershov Institute of Informatics Systems. Retrieved from: https://www.iis.nsk.su/files/articles/sbor_kas_16.pdf.

14. Mirzaev, N. M. (2012). Model' vydeleniya priznakov v zadache diagnostiki fitosostoyaniya rasteniy po izobrazheniyam list'yev [Feature extraction in the problem of diagnozing of plants' phytocondition by leaves' images] (in Russian). *Vestnik Ryazanskogo gosudarstvennogo radiotekhnicheskogo universiteta [Vestnik of Ryazan State Radio Engineering University], 3*(41), 21–25.

15. Zhuravlev, Yu. I. (1998). *Izbrannyye nauchnyye trudy [Selected papers]* (in Russian). Moscow, Russia: Magistr.

16. Mirzaev, N. M. (2010). About one model of image recognition. *Computer Technology and Applications: Proceedings of The First Russia and Pacific Conference* (pp. 394–398). Vladivostok, Russia.

17. Gonzales, R., & Woods, R. (2008). *Digital image processing.* New Jersey, USA: Prentice Hall.

18. Fazilov, Sh. Kh., Mirzaev, N. M., & Mizraev, O. N. (2016). Postroyeniye raspoznayushchikh operatorov v usloviyakh vzaimosvyazannosti priznakov [Building of recognition operators in condition of features' correlations] (in Russian). *Radioelektronika, informatika, upravleniye [Radio Electronics, Computer Science, Control], 1*(36), 58–63. Retrieved from: http://nbuv.gov.ua/UJRN/riu_2016_1_9.

19. Kamilov, M. M., Fazilov, Sh. Kh., Mirzaev, N. M., & Radjabov, S. S. (2012). Estimates calculations algorithms in condition of huge dimensions of feartures' space. *Problems of Cybernetics and Informatics (PCI'2012): Proceedings of the 4th International Conference, vol. I* (pp. 184–187). Baku, Azerbaijan.

20. Braga-Neto, U. M., & Dougherty, E. R. (2016). *Error estimation for pattern recognition.* New York, USA: Springer.

Optimal Location of Biogas Complexes in the Region

D. G. Nefedov [1], E. V. Kasatkina [2]

Dept. of Mathematical Support for Information Systems, Kalashnikov Izhevsk State Technical University,
Izhevsk, Russian Federation
E-mail: [1] denisnefedov1@yandex.ru, [2] e.v.trushkova@gmail.com

Abstract. The report provides the application of biogas technologies at livestock enterprises as a complex solution of alternative energy supply of heat sources on natural gas. The organization of biogas complexes is a high-cost event and requires the selection of the optimal location variant, which consists in minimizing the total costs associated with the production of biogas and its delivery to consumers. Optimization is based on the construction of mathematical models for the location of elements of a distributed production structure. The method of solving this problem is based on the use of a genetic algorithm with real coding and the use of parallel computations. In this paper, an example of the solving the problem of the optimal location of biogas complexes in the territory of the Udmurt Republic of Russian Federation is presented. The estimation of the economic effect of substitution of natural gas with biogas is given, the optimal volume of its production is determined taking into account the solution of the ecological problem of processing livestock wastes and the possibility of selling by-products from biogas production. The results of the calculations are presented in graphical and tabular form.

Keywords: biogas complex, facility location, intermediate production, final product, genetic algorithm.

INTRODUCTION

The distributed industrial structure is typical for many branches of industry and agriculture associated with the production and recycling of various types of raw materials and minerals [1]. This industry also includes the production of biogas from animal wastes [2, 3]. The construction of mathematical models and tools for calculating the optimal production structure and facility location for processing raw materials into products allows the most rational use of available resources and, accordingly, to achieve the best values of the placement performance index, which consists in minimizing costs or maximizing profits [4].

Problems of mathematical modeling of facility location at the modern level are devoted to the works of M. Daskin, Z. Drezner, S. Hakimi, R. Churche and others [5]. They describe various location models taking into account the multilevel and multiproduct nature of production, time and probabilistic parameters, restrictions on the output. Methods for solving the problems of facility location are described in M. Fisher, R. Galvao, S. Revile, B. Bockaya, J. Zhang, E. Erkut, J. Bramell, E. Rolland, K. Rosing [6, 7].

The meaningful formulation of the problem of allocating elements of a distributed production structure is as follows (see Figure 1).
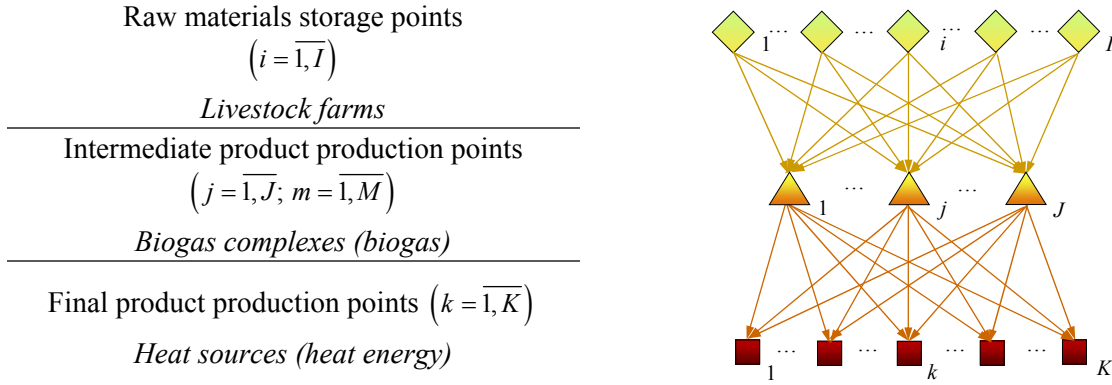
Figure 1. Scheme of interrelation of raw materials storage points,
intermediate product production points and final product production points

There are a number of K production points for the final product. To produce it, M interchangeable types of intermediate products are used. For its production, raw materials are used, prepared in raw material storage points, the total number of which is equal to I. It is required to find the volumes of output of intermediate products in each of J potential points of its production. Possible positions of intermediate products manufactured points are determined in advance, and they may or may not coincide with the location of the storage points of raw materials and points of the final product production [8].

MATHEMATICAL MODEL

The mathematical model of considered problem is based on the methodology for calculating the cost of intermediate production and the final product, given in [9, 10].

The objective function of the problem is to minimize the total costs for the final product, taking into account the costs of production and delivery of intermediate products:

$$C = C^{IP} + C^{FP} \to \min, \tag{1}$$

$$C^{IP} = \sum_{j=1}^{J} \sum_{m=1}^{M} F_j^m \left(V_j^m \right) + \sum_{i=1}^{I} \sum_{j=1}^{J} \sum_{k=1}^{K} \sum_{m=1}^{M} \tau^m \left(\alpha^m g_{ij}^m + g_{jk}^m \right) x_{ijk}^m D_k, \tag{2}$$

$$C^{FP} = \sum_{k=1}^{K} \sum_{m=1}^{M} E_k^m \left(D_k^m \right), \tag{3}$$

where C are total costs for production of intermediate and final products, rub./year; C^{IP} are costs for transportation of raw materials, production of intermediate products and its delivery to the final product production points, rub./year; C^{FP} are costs for processing intermediate products into the final product at production points, rub./year; V_j^m is the output of m-th type of intermediate products at the j-th production point, un.i.p./year; D_k is the output of the final product at the k-th production point, un.f.p./year; D_k^m is the output of the final product at the k-th production point on the m-th type of intermediate products, un.f.p./year; $F_j^m \left(V_j^m \right)$ are costs of processing raw materials into the m-th type of intermediate products at the j-th production point, rub./year; $E_k^m \left(D_k^m \right)$ are costs for processing m-th type of intermediate produc-

tion into the final product at the k-th production point, rub./year; g_{ij}^m are costs of transporting a unit of raw materials used to produce the m-th type of intermediate production, between the i-th raw materials storage point and j-th point of its production, rub./un.r.m.; g_{jk}^m are costs of transporting a unit of m-th type of intermediate production between the j-th point of its production and the k-th point of final product production, rub./un.i.p.; x_{ijk}^m are managed variables that determine a share of the final product from the k-th point of its production, produced in the m-th type of intermediate production from the j-th point of its production with the consumption of the raw materials from the i-th storage point.

The costs of processing of raw materials into the intermediate production $F_j^m\left(V_j^m\right)$ are determined on the basis of technical and economic calculation:

$$F_j^m\left(V_j^m\right) = a_j^m V_j^m + b_j^m \Theta\left(V_j^m\right), \; j = \overline{1,J}, \; m = \overline{1,M}, \tag{4}$$

where a_j^m are the conditional-constant costs per unit of the m-th type of intermediate production output at the j-th point of its production, rub./un.i.p.; b_j^m are the conditional-constant costs for the entire output of the m-th type of intermediate production at the j-th point of its production, rub./year; $\Theta\left(\chi\right)$ is Heaviside function.

The costs of processing of intermediate production into the final product are

$$E_k^m\left(D_k^m\right) = \tilde{a}_k^m D_k^m + \tilde{b}_k^m \Theta\left(D_k^m\right), \; k = \overline{1,K}, \; m = \overline{1,M}, \tag{5}$$

where $\tilde{a}_k^m$ are the conditional-constant costs per unit of the final product at the k-th point of its production on the m-th type of intermediate production, rub./un.f.p.; $\tilde{b}_k^m$ are the conditional-constant costs for the entire output of the final product at the k-th point of its production on the m-th type of intermediate production, rub./year.

The following relationships are accepted as the restrictions:

$$V_j^m = \tau^m \sum_{i=1}^I \sum_{k=1}^K x_{ijk}^m D_k, \; j = \overline{1,J}, \; m = \overline{1,M}; \tag{6}$$

$$D_k^m = D_k \sum_{i=1}^I \sum_{j=1}^J x_{ijk}^m, \; k = \overline{1,K}, \; m = \overline{1,M}; \tag{7}$$

$$\alpha^m \tau^m \sum_{j=1}^J \sum_{k=1}^K x_{ijk}^m D_k \leq W_i^m, \; i = \overline{1,I}, \; m = \overline{1,M}; \tag{8}$$

$$\sum_{i=1}^I \sum_{j=1}^J \sum_{m=1}^M x_{ijk}^m = 1, \; k = \overline{1,K}; \tag{9}$$

$$x_{ijk}^m \in \left[0; 1\right], \; i = \overline{1,I}, \; j = \overline{1,J}, \; k = \overline{1,K}, \; m = \overline{1,M}. \tag{10}$$

where W_i^m is the volume of raw materials at the i-th point of accumulation, used to produce the m-th type of intermediate production, un.r.m./year.

Relations (6), (7) establish a balance between the output of intermediate production at its production points and demand for it at the final product production points. Expression (8) determines the balance between the required volume of raw materials and the potential of the raw materials base at the points of its accumulation. The constraint (9) reflects the condition

for the satisfaction all the final product production point with the intermediate production. The restriction (10) shows the domain of the desired solution.

NUMERICAL SOLUTION ALGORITHM

The presented mathematical model belongs to the class of problems of nonlinear optimization [11]. In this case, the search for the optimal solution is complicated by the large dimension of the vector of the desired solutions. The specificity of the problem (1)–(10) is the inability to differentiate the objective function. Therefore, the main problem is the choice of the method for the numerical solution of the optimization problem.

The method for solving this problem is based on a genetic algorithm with real coding. A block diagram of this algorithm using parallel computations is presented in Figure 2.
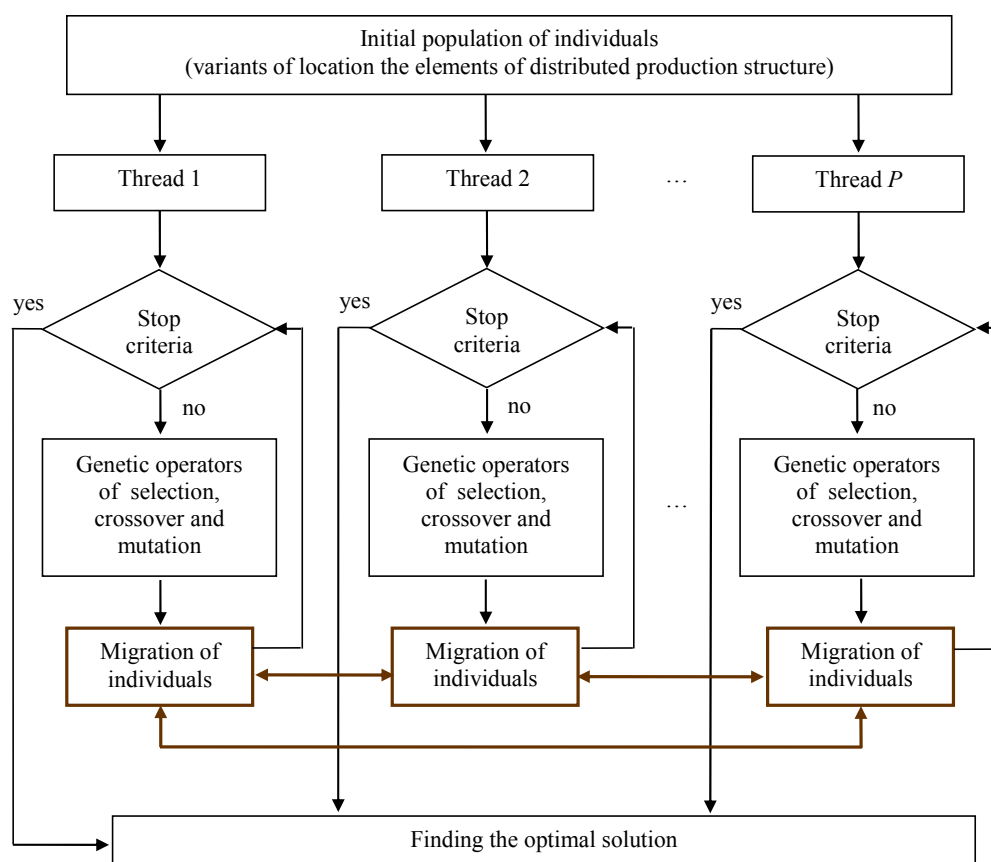
Figure 2. Block diagram of genetic algorithm using parallel computations

Search for solution of the problem involves several stages:
1. Formation of the initial population of individuals.
2. Assessment of fitness of individuals.
3. Application of genetic operators. Over individuals within each flow, the action of genetic operators is carried out: selection, crossover and mutation.
4. Migration of individuals. At this stage, there is a movement of individuals from one thread to another – migration is carried out.
5. Finding the optimal solution of the problem. The best individual of a given thread is compared to the best individuals of the remaining threads, and the winner becomes the solution of the problem.

The partitioning of the population into several threads and the execution of intra-thread operations by individual processors of the computing device leads to a significant increase in the overall speed of searching for the optimal solution.

OPTIMAL LOCATION SCHEME FOR THE BIOGAS COMPLEXES ON THE TERRITORY OF UDMURT REPUBLIC

In Udmurt Republic in 2015, more than 50 % of the animal wastes were provided by the 60 livestock farms [12, 13]. They are chosen as potential locations for biogas complexes. 383 heat sources have been chosen as potential biogas consumption points [14]. The organization of biogas complexes is a high-cost event, and the cost of biogas and heat energy on biogas is reduced due to large volume of production that can be achieved by using the raw materials from large livestock enterprises. Further increase in production is achieved at the expense of smaller enterprises. This leads to a parametric problem of determining the largest economically feasible volume of biogas production, in which the total cost of heat energy on biogas, including the cost of its production, does not exceed the cost of heat energy on natural gas, including the cost of its purchase. To solve the problem, the above mathematical model is used, in which the optimization criterion is minimization of the cost of heat energy on biogas subject to a given volume of production. Figure 3 shows the optimal values of objective function C – the cost of heat energy – for each of the given volumes of biogas production V^{bg}. In the same figure, for comparison, an analogous dependence is given for the cost of heat energy on natural gas. The increase in biogas production due to smaller livestock enterprises leads to an outpacing increase in the cost of biogas as compared to the fixed cost of natural gas, which also affects the cost of heat energy.
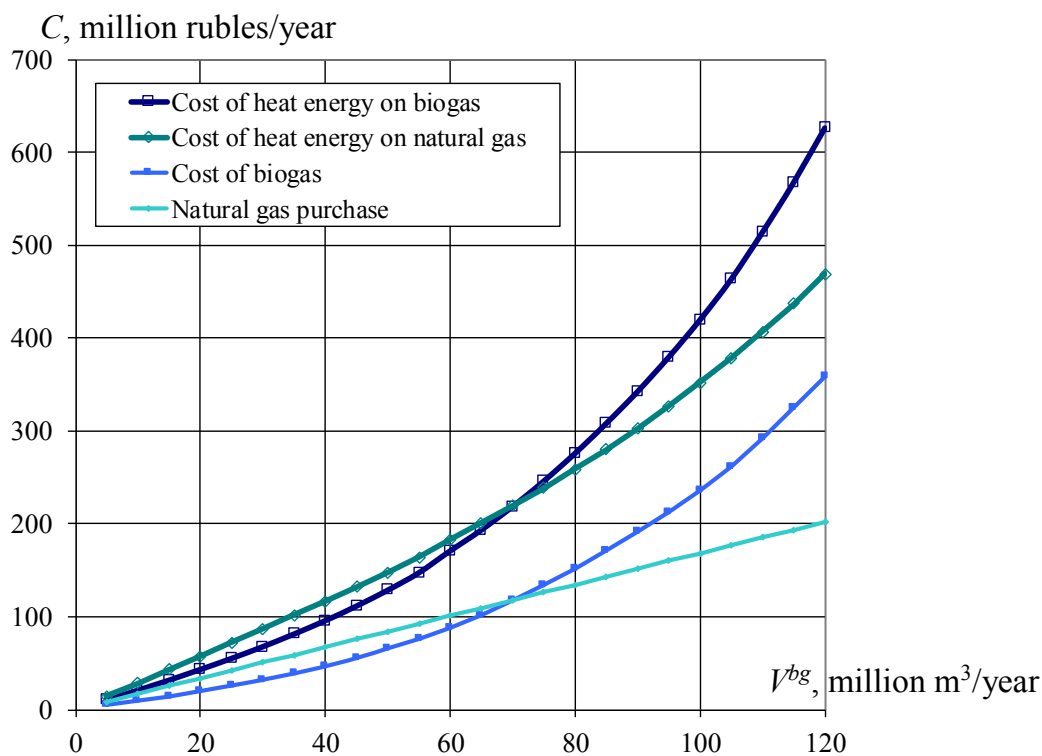
Figure 3. Dependence of the cost of heat energy production on biogas and natural gas from total biogas production

The presented results show that with $V^{bg} > 70$ million m³ / year the use of biogas to replace them natural gas under the conditions of the Udmurt Republic is economically unprofitable. The optimal scheme of facility location corresponding to the volume of 70 million m³ of biogas per year includes 16 biogas complexes located near the largest livestock enterprises supplying 62 heat sources (see Figure 4).
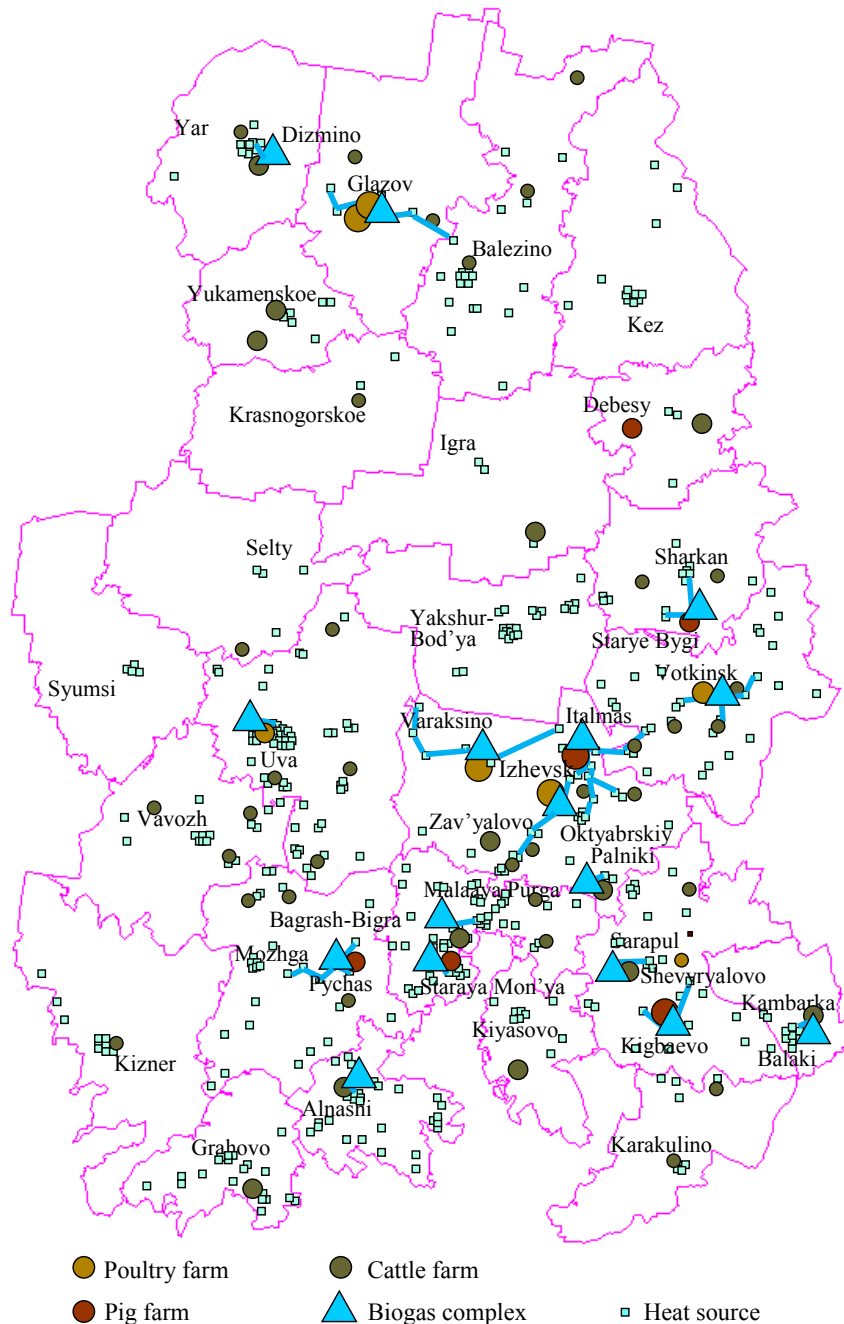

Figure 4. Optimal location of biogas complexes

Volumes of biogas production on biogas complexes are given in Table 1. As calculations have shown, in this case the total costs for the production of heat energy including fuel costs will be 215 million rubles per year. The average cost of production of heat energy on biogas for selected heat sources will be equal to 701 rubles / Gcal.

Table 1. Biogas complexes in Udmurt Republic

No	Location of biogas complex	Volume of biogas production, million m^3/year	Number of heat sources supplied
1	Italmas	21.53	12
2	Varaksino	11.20	6
3	Glazov	8.21	5
4	Oktyabrskiy	5.77	4
5	Kigbaevo	5.07	3
6	Votkinsk	2.66	5
7	Pychas	2.65	5
8	Dizmino	2.29	3
9	Alnashi	2.08	2
10	Uva	1.82	3
11	Balaki	1.67	2
12	Bagrash-Bigra	1.38	2
13	Palniki	1.17	1
14	Shevyryalovo	0.97	3
15	Starye Bygi	0.85	3
16	Staraya Mon'ya	0.73	3
	Total	**70.05**	**62**

Figure 5 shows the dependence of the annual economic effect E obtained by the substitution of natural gas with biogas on heat sources, on the volume of biogas production. Its value is determined by the difference between the total costs for the heat energy production on natural gas and biogas.
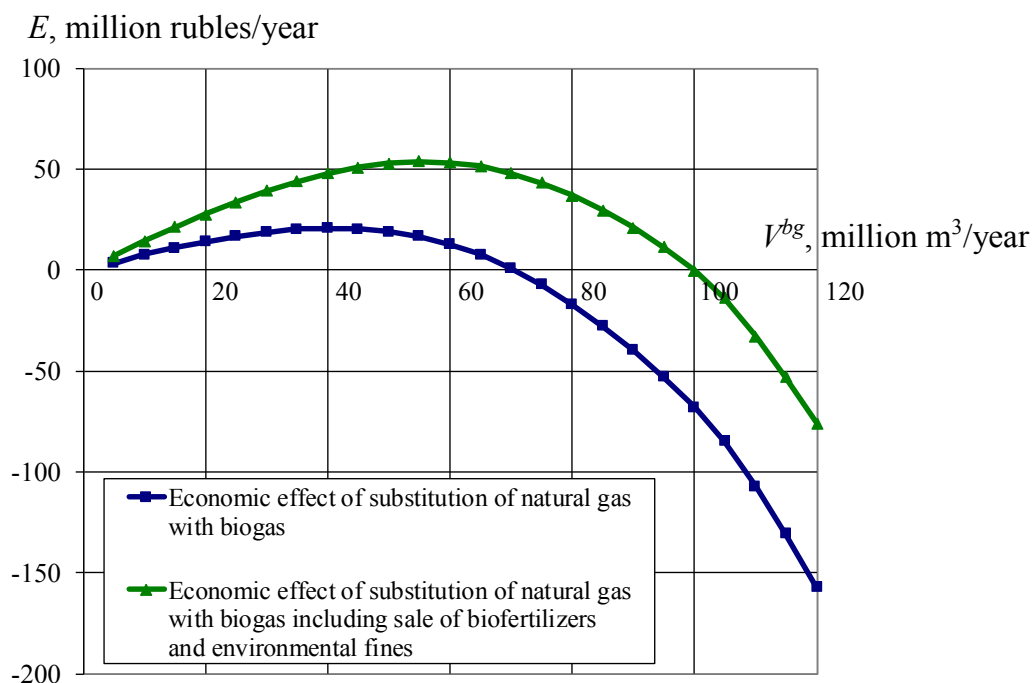
Figure 5. Dependence of the annual effect on substitution of natural gas with biogas of the total volume of its production

The biogas production yields the ecologically clean organic fertilizers. In addition, the waste of livestock enterprises, according to the classification of the Ministry of Natural Resources and Ecology of the Russian Federation, is a hazard class III substance, the utilization of which in the production of biogas allows the elimination of environmental fines. Taking into account the income from the sale of solid biofertilizers at a cost of 500 rubles per ton and exclusion of environmental fines equal to 100 rubles per ton of dry matter, economically profitable biogas production in Udmurt Republic increases from 70 to 100 million m^3 per year, and the maximum economic effect increases from 20 to 55 million rubles per year.

CONCLUSION

As a result of solving the problem of optimizing the location of biogas complexes in the territory of the Udmurt Republic it is determined that the maximum amount of biogas production, at which it is economically feasible to replace natural gas, is 70 million m^3 per year. For this volume, the optimal number and location of biogas complexes supplying 62 heat sources is given. Taking into account the income from the sale of biofertilizers and the exclusion of environmental fines, economically profitable output of biogas increases to 100 million m^3 per year.

REFERENCES

1. Rusyak, I. G., Ketova, K. V, & Trushkova, E. V. (2011). Logistic task of fuel supply for the regional distributed heat supply system. *Journal of Knowledge Management, Economics and Information Technology,1*(7), 445–477. – Retrieved from: http://www.scientificpapers.org/wp-content/files/1235_Ekaterina_Trushkova_Logistic_Task_of_Fuel_Supply_for_the_Regional_Distributed_Heat_Supply_System.pdf.

2. Budiyono, I. N., & Widiasa, S. J. (2010). Increasing biogas production rate from cattle manure using rumen fluid as inoculums. *International Journal of Basic & Applied Sciences IJBAS-IJENS, 10*(1), 68–74. doi:10.12777/ijse.6.1.31-3.

3. Balussou, D., Heffels, T., McKenna, R., Möst, D., & Fichtner, W. (2014). An evaluation of optimal biogas plant configurations in Germany. *Waste and Biomass Valorization, 5*(5), 743–758. doi:10.1007/s12649-013-9284-1.

4. Daskin, M. S. (2008). What you should know about location modeling. *Naval Research Logistics, Economics and Information Technology, 55*(4), 283–294. doi:10.1002/nav.20284.

5. Daskin, M. S. (2011). *Network and discrete location: models, algorithms, and applications.* New York, USA: Wiley. doi:10.1002/9781118032343.

6. Bozkaya, B., Zhang, J., & Erkut, E. (2002). An efficient genetic algorithm for the p-median problem. In Z. Drezner, H. W. Hamacher (Eds.), *Facility location: applications and theory* (pp. 179–205). Berlin, Germany: Springer.

7. Price, K., Storn, R., & Lampinen, J. (2005). *Differential evolution: a practical approach to global optimization.* Berlin, Germany: Springer.

8. Rusyak, I. G., & Nefedov, D. G. (2012). Reshenie zadachi optimizacii shemy razmeshcheniya proizvodstva drevesnyh vidov topliva po kriteriyu sebestoimosti teplovoj energii [Solution of optimization problem of wood fuel facility location by the thermal energy cost criterion]. *Komp'yuternyye issledovaniya i modelirovaniye [Computer Research and Modeling], 4*(3), 651–659 (in Russian).

9. Rusyak, I. G., Ketova, K. V., & Nefedov, D. G. (2017). Matematicheskaya model' i metod resheniya zadachi optimal'nogo razmeshcheniya proizvodstva drevesnyh vidov topliva [Mathematical model and method for solving problem of optimal location of wood fuels facility]. *Izvestiya Rossiyskoy Akademii Nauk. Energetika [Proceedings of the Russian Academy of Sciences. Power Engineering], 2017*(2), 177–187 (in Russian).

10. Rusyak, I. G., Presnukhin, V. K., Ketova, K. V., Korolev, S. A., & Trushkova, E. V. (2010). Razrabotka koncepcii toplivoobespecheniya raspredelennoj regional'noj sistemy teplosnabzheniya mestnymi vozobnov-lyaemymi vidami topliva [Development of the concept of fuel supply distributed regional heating system of local renewable fuels]. *Energobezopasnost` i Energosberezhenie [Energy Safety and Energy Economy], 2010*(5), 14–20 (in Russian).

11. Ruszczyński, A. (2006). *Nonlinear optimization.* Princeton, NJ, USA: Princeton University Press.

12. Korolev, S. A., Valiullin, M. A., Merzlyakov, A. Yu., & Sairanov, A. S. (2013). Analiz potenciala vozobnov-lyaemyh istochnikov energii Udmurtskoj Respubliki [Analysis of the renewable energy potential of the Udmurt Republic]. *Intellektual'nye Sistemy v Proizvodstve [Intelligent Systems in Manufacturing], 2013*(2), 194–198 (in Russian).

13. Korolev, S. A., & Maykov, D. V. (2011). Vliyanie klimaticheskih uslovij na teplovoj rezhim raboty biogazo-voj ustanovki [Influence of climatic conditions on the thermal mode of a biogas plant]. *Bulletin of Kalash-nikov ISTU, 2011*(2), 209–213 (in Russian).

14. Korolev, S. A., & Maykov, D. V. (2013). Informacionno-analiticheskaya sistema proektirovaniya structury, rascheta i optimizacii tehnologicheskih i economicheskih parametrov biogazovyh kompleksov [Information-analytical system of structure design, calculation and optimization of technological and economic parameters of biogas complexes]. *Intellektual'nye Sistemy v Proizvodstve [Intelligent Systems in Manufacturing], 2013*(2), 198–202 (in Russian).

Photonic Applications and their Coexistence with Standard Data Transmissions

J. Radil, T. Horvath, P. Munster, O. Havlis, P. Skoda, V. Smotlacha, J. Vojtech

Optical Networks Department, CESNET z.s.p.o., Praha, Czech Republic
E-mail: jan.radil@cesnet.cz

Abstract. Fibre networks are rather common today almost in many parts of the world and it looks that fibre as the transmission medium is here to stay for some time. Data transmissions in the backbone fibre networks are based on coherent detection principles and use multilevel phase modulations like quadrature phase shift keying used for 100 Gb/s transmission speeds. But there are also new photonic applications with different requirements then raw speeds only. In order to guarantee seamless coexistence of standard and new photonic applications, we evaluate numerical simulations by using commercially available simulation tools. The simulations results show that such coexistence is possible when certain rules are followed. Simulation results are verified on real fibres to ensure reliable operation.

Keywords: fibre sensors, accurate time transfer, ultra stable frequency transfer, coherent transmission, high speed transmission.

INTRODUCTION

High speed data networks using standard single mode fibres (SSMF) are used to transfer huge amount of data between continents for good few years now. Coherent receiver principles and multilevel modulation formats can offer transmission speeds up to 400 Gb/s, with help of 64-level quadrature amplitude modulation (64QAM), in one dense wavelength division multiplexing (DWDM) channel.

But there are also other applications utilizing optical fibre called Photonic applications or services. Examples of such applications are accurate time transfer, ultra stable frequency transfer or fibre sensing and transmission speeds are not important anymore but rather minimal and constant delay or jitter and no vibrations.

National research and educational network (NREN) are pioneers of new developments in rather unexplored areas of research networking and special requirements for new applications were collected and described for example in [1] and [2].

PHOTONIC (NON-DATA) APPLICATIONS

New applications like accurate time transfer and ultra-stable frequency are not as exotic as they were just few years ago and their potential for sensing, metrology, navigation, seis-

mology or fundamental physics is accepted these days. Another fresh area of new applications is using of optical fibre for sensing.

Such non-data signals are usually amplitude modulated (or even not modulated at all which is the case for ultra-stable frequency transfer where the transmitted information is the frequency of photons) with rather slow speeds and new challenges certainly will arise when such non-data and high speed data signals are transmitted together in one fibre. And one fibre (or fibre infrastructure to be precise) must be shared by all such signals because it is not possible to deploy one fibre infrastructure for data, one for sensing applications and one for time and/or frequency transfer. The reasons are economical because no operator can afford to build and pay completely independent long haul fibre networks for every photonic application. This situation may be different in certain networking environments, for example Data Centre Interconnects (DCI) where optical cables with up to few thousands individual fibres may be installed and used independently.

Sensing (using fibre as a sensor) applications, for example phase sensitive optical time domain reflectometry (phi-ODTR) do use high optical powers which may influence phase modulated high speed data signals, especially via nonlinear mechanism of cross phase modulation (CPM). Phase sensitive OTDR is de facto slow amplitude modulated signal in its simplest form, known as on-off keying modulation (OOK). This is the reason that simultaneous transmission of such sensing signals is an important research area because coherent transmission systems can compensate for phenomenons like chromatic dispersion (CD) or even stochastic polarization mode dispersion (PMD) but today cannot cope with nonlinear effects like CPM or four wave mixing (FWM), described in detail in [3]. The reason that nonlinear effects cannot be compensated easily is complex mathematics of course.

It is clear that most demanding of photonic applications is sensing - because of relatively high optical powers launched into the fibre. Accurate time signals are also amplitude modulated but optical powers are similar to powers used for coherent data signals. And ultra stable frequency transfer is not modulated and also not as powerful as sensing signals, therefore possible mutual interference with data signals is relatively modest, however it is important to include them in practical verification because of optical amplifiers conditions like tampering with gain and output powers. Accurate time transfer results can be found in [4] and [5]. Ultrastable frequency transfer is described in [6] and [7]. Fibre sensing review can be found in [8] and some latest results in [9].

PRACTICAL RESULTS

For reasons mentioned in the previous section, simultaneous transmission of high speed coherent signals and high-power phase sensitive reflectometry signals, together with accurate time and ultra stable frequency, was performed in lab environment on fibre spools. We started experiments with shorter distances below 10 km of fibre and measurements were performed both with G.652 and G.655 fibres because both types of fibres are used in the CESNET network. Multiplexing and demultiplexing (or filtering) was realized on the standard 100 GHz ITU grid. Some previous results can be found in [10] and [11].

Detailed measurement scheme showing both data and non-data applications is depicted in Figure 1. As can be seen, each service uses the wavelength according to the ITU DWDM 100 GHz grid. The goal was to prove simultaneous transmissions in one fibre and with the standard channel spacing 100 GHz (according to ITU). Requirement on the standard channel spacing is because in some cases is not possible to use whole spectrum but only dedicated

DWDM channel for multiple services. Accurate time transfer (1550.12 nm), frequency transfer (1552.52 nm), and 100G data (1551.72 nm) were multiplexed together in a standard telecommunication multiplexer.

All multiplexed signals are sent to the phi-OTDR, then the sensing signal is mixed and all signals are launched into a fibre spool. This configuration allows loss minimization of the sensing signal.
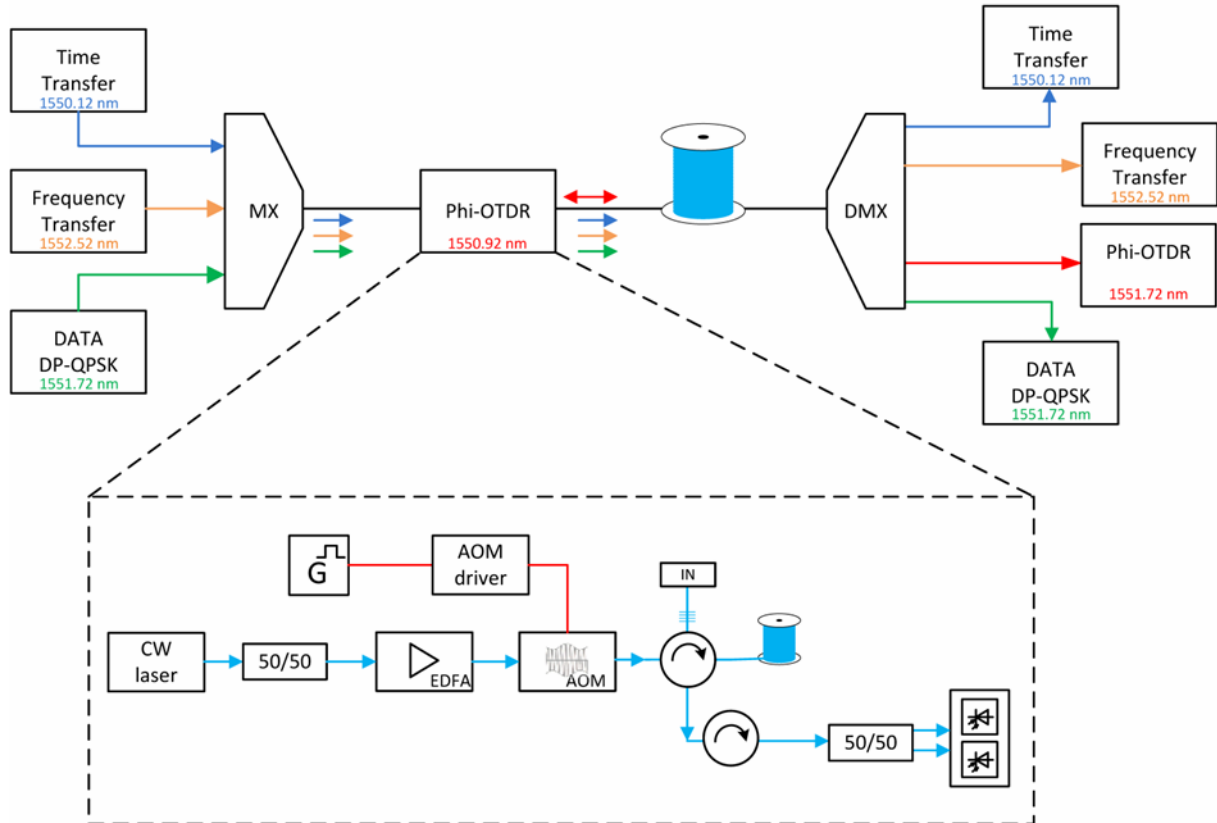
Figure 1. Set-up for laboratory measurements for accurate time, stable frequency, phi-OTDR and coherent signals

The experiments were performed for G.652 and G.655 fibres because such fibres are usually deployed in fibre optic networks – this is true for the CESNET backbone optical network. Some experiments were performed with G.653 fibre which may be considered as rather rare but we believe it is still useful for real comparison of three different fibres.

Important aspect was different duration of phi-OTDR pulses – 20 ns, 200 ns and 2000 ns, with the same and constant repetition rate 5 kHz. As expected, G.652 fibre is more resistant to higher launched optical powers due to bigger effective core area.

Figure 2 and Figure 3 show results for three different types of fibres and dependency of bit error rate (BER) of 100 Gb/s coherent data signal on pulsed sensing signals with different optical output powers launched into the fibre.

We can see that 200 ns and 2000 ns curves crossing for higher powers – this can be caused by small time intervals for measurements and also sensing pulses are sometimes overlapping with data signals more (it is a random process). G.653 has even smaller effective area compared to G.655 so tolerance to optical powers is smaller as can be seen on Figure 3.
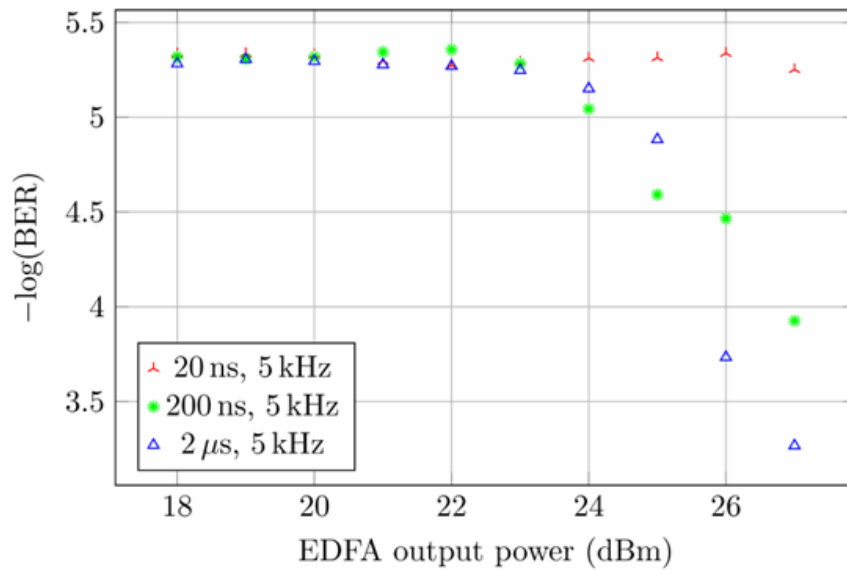
Figure 2. Dependence of 100 Gb/s data signal on sensing signal for G.652+G.655 fibres
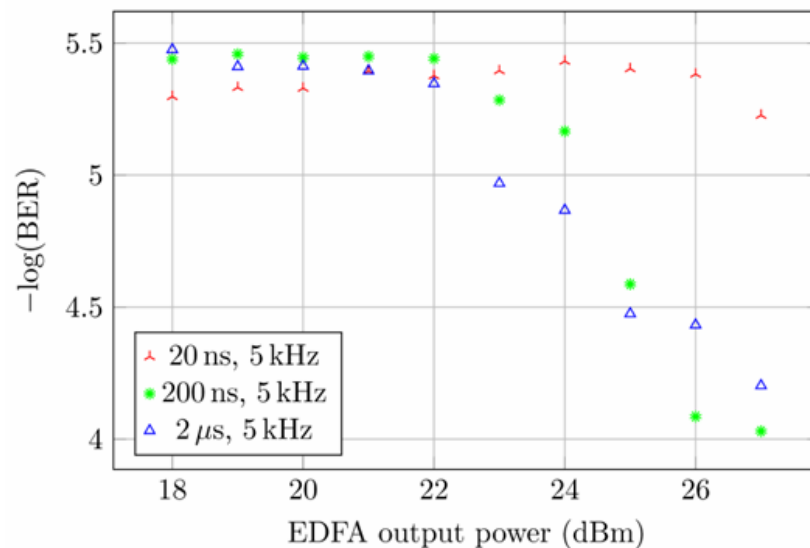

Figure 3. Dependence of 100 Gb/s data signal on sensing signal for G.652+G.653 fibres
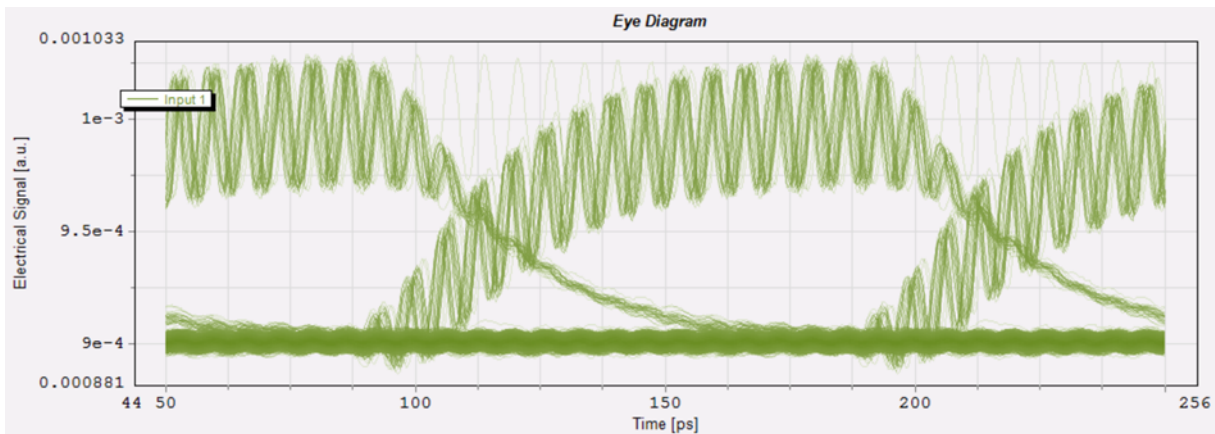
NUMERICAL SIMULATIONS

Numerical simulations are important part of this work. VPI photonics software was used to simulate optical data networks, sensing elements and transmission systems. Two different modulation formats (OOK, QPSK), three different transmission speeds (1, 10 and 100 Gb/s) and various optical powers were used to verify nonlinear thresholds especially for CPM.

Different interferometric methods which are used for sensing applications were simulated. Three most important and also practically deployed methods use Mach-Zehnder, Michelson and Sagnac interferometres.

Two examples of simulations results are depicted in Figure 4 and Figure 5, showing the eye diagrams for 10 Gb/s data signals and sensing pulse signals. As can be seen the difference between 50 GHz and 150 GHz adjacent-channel spacing is rather visible.
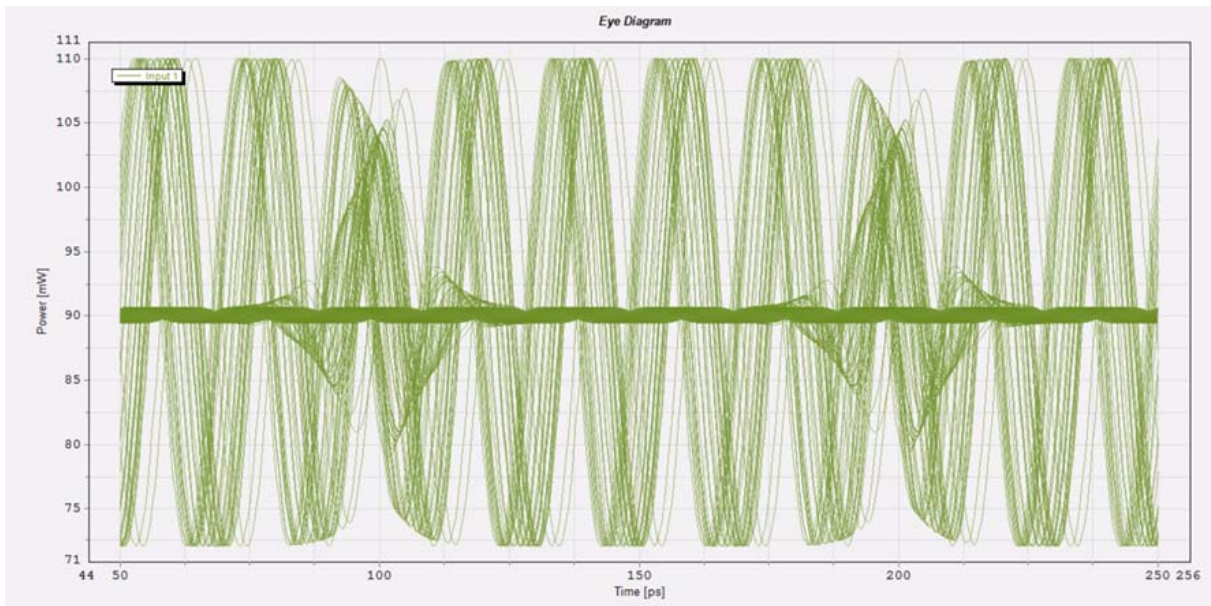
Figure 4. Eye diagrams for 10 Gb/s and sensing signals for 50 GHz channel spacing

Figure 5. Eye diagrams for 10 Gb/s and sensing signals for 150 GHz channel spacing

CONCLUSION

We have verified the real coexistence of different applications in one fibre, based on previously performed numerical simulations. Verification was performed on two types of fibres deployed in the CESNET network – G.652 and G.655, with different pulse durations of phi-OTDR sensing signals. Obviously that more powerful sensing pulses are, the worse degradation of data signals is observed.

We have found that real results measured on real optical systems are different than simulation results. One reason for this discrepancy can be that simulation software could not take into account all subtleties of all components used (e.g. phase difference for different fused fibre couplers). Also simulation software is designed mostly for data communications and not for special sensing applications.

But results indicate that simultaneous transmission of standard high speed coherent data signals and high-power sensing signals is possible without any serious consequences. This is very promising because such new sensing applications can be deployed not only in NRENs but also in commercial operational networks.

ACKNOWLEDGMENTS

REFERENCES

1. Altmanova, L. et al. (2013). Photonic services: challenge for users and for networkers. *The GN3 project report.*

2. Vojtech, J., Smotlacha, V., Skoda, P., Kuna, A., Hula, M., Sima, S. (2012). Photonic services, their enablers and applications. In *Proceedings SPIE Volume 8516, Remote Sensing System Engineering IV,* 85160H. doi:10.1117/12.929908.

3. Agrawal, G. P. (2010). *Fiber-optic communication systems* (4th ed.). New York, USA: Wiley.

4. Emardson, R., Hedekvist, P. O., Nilsson, M., Ebenhag, S.-C., Jaldehag, K., Jarlemark, P., Rieck, C., Johansson, J., Pendrill, L. R., Lothberg, P., & Nilsson, H. (2008). Time transfer by passive listening over a 10-Gb/s optical fiber. *IEEE Transactions on Instrumentation and Measurement, 57*(11), 2495–2501. doi:10.1109/TIM.2008.925023.

5. Zhang, H., Wu, G., Hu, L., Li, X., & Chen, J. (2015). High-precision time transfer over 2000-km fiber link. *IEEE Photonics Journal, 7*(6), 1–9, doi:10.1109/JPHOT.2015.2499541.

6. Predehl, K., Grosche, G., Raupach, S. M. F., Droste, S., Terra, O., Alnis, J., Legero, T., Hänsch, T. W., Udem, T., Holzwarth, R., & Schnatz, H. (2012). A 920-kilometer optical fiber link for frequency metrology at the 19th decimal place. *Science, 336*(6080), 441–444. doi:10.1126/science.1218442.

7. Lopez, O., Haboucha, A., Chanteau, B., Chardonnet, C., Amy-Klein, A., & Santarelli, G. (2012). Ultra-stable long distance optical frequency distribution using the Internet fiber network. *Optics Express, 20*(21), 23518–23526. doi:10.1364/OE.20.023518.

8. Thévenaz, L. (2006). Review and progress on distributed fibre sensing. In *Optical Fiber Sensors 2006, OSA Technical Digest (CD)*, paper ThC1. Cancun, Mexico: Optical Society of America. doi:10.1364/OFS.2006.ThC1.

9. Schenato, L., Palmieri, L., Camporese, M., Bersan, S., Cola, S., Pasuto, A., Galtarossa, A., Salandin, P. & Simonini, P. (2017). Distributed optical fibre sensing for early detection of shallow landslides triggering. *Scientific Reports, 7*(article number: 14686), 1–7. doi:10.1038/s41598-017-12610-1.

10. Munster, P., Horvath, T., Havlis, O., Vojtech, J., Radil, J., Velc, R., & Skaljo, E. (2017). Simultaneous transmission of standard data, precise time, stable frequency and sensing signals and their possible interaction. In *Proceedings of SPIE, 10231, Optical Sensors 2017,* 102312A. doi:10.1117/12.2266240.

11. Vojtech, J., Slapak, M., Skoda, P., Radil, J., Havlis, O., Altmann, M., Munster, P, Velc, R., Kundrat, J., Altmannova, L., Vohnout, R., Horvath, T., Hula, M., Smotlacha, V., Cizek, M., Pravdova, L., Rerucha, S., Hrabina, J., & Cip, O. (2017). Joint accurate time and stable frequency distribution infrastructure sharing fiber footprint with research network. *Optical Engineering, 56*(2), 027101. doi:10.1117/1.OE.56.2.027101.

Defectoscopy of Composite Fiberglass Fittings by the Acoustic Waveguide Technique

V. A. Strizhak [1], S. S. Mkrtchyan [2], R. R. Khasanov [3], A. V. Pryakhin [4], A. B. Efremov [5]

Department of Measuring, Testing, Diagnostic Instruments and Techniques,
Kalashnikov Izhevsk State Technical University, Izhevsk, Russian Federation
**E-mail: [1] str@istu.ru, [2] sergsmile@yandex.ru,
[3] beif@mail.ru, [4] 1814nrt@mail.ru, [5] rushaggy@gmail.com**

Abstract. In this paper we propose the procedure of non-destructive testing of composite fiberglass reinforcements by using the acoustic waveguide technique. Experiments on defectoscopy of the composite armature with rod waves were conducted. More than 1000 composite fiberglass reinforcements with length of 6 meters were tested according to the developed procedure. The experimental results shown that rejection level of 2 % allows to detect, confirm and identify flaws by type. Furthermore, we derived the dependence between signal amplitude and discontinuities or changes in the cross-section of the composite reinforcement body. The simulation of flaw as an element with a cross-sectional difference was performed. A graphical dependence of the signal amplitude from the flaw and from the defect zone cross-sectional area value was obtained. The photographs of typical defects and the corresponding echograms are given in this paper.

Keywords: acoustic non-destructive testing, waveguide technique, defectoscopy, development of procedure, composite fittings.

INTRODUCTION

In the construction industry, composite fittings has recently been increasingly used (Figure 1). It has a relatively low cost compared to metal fittings and better serviceability, while the manufacturing process is simpler. Composite fittings do not have a negative impact on human health.

In connection with the anisotropic properties of the material, high attenuation coefficient, a large amount of processing deficiency, low quality of the components included in the material, non-destructive testing (NDT) of the composite fittings is a difficult process. The quality of buildings and structures directly depends on the quality of the composite fittings. The use of low-quality fittings can result in death or injury to people [1–2].

Most NDT methods based on electromagnetic phenomena and are not applicable to composite materials testing. The problem is the lack of methods for non-destructive testing of such products [3–5]. However, testing of this type of fittings is possible using the acoustic guided wave method.
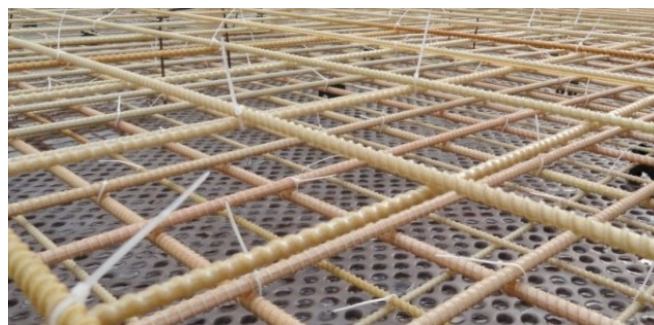
Figure 1. Composite fiberglass fittings

The most interesting is the implementation of testing technology for composite fittings using guided waves. The technology of acoustic guided wave testing can be implemented for extended objects, which length many times exceeds the dimension of the cross-sections [6–12]. Guided wave technique has been successfully implemented in non-destructive testing of bars, pump compressors rods, sucker rods, tubings, fluid level measurement in wells, etc. [13–15].

Advantages of the technique:

- does not require the use of contact and immersion liquids, any preparation of the surface of the object of testing;
- sensitivity to defects throughout the cross-section of the bar;
- no need to scan;
- possibility of testing at local access to the flat end of the object;
- high productivity;

The rod wave used is characterized by a small dispersion of the velocity peculiar to the other Pochhammer types of waves [6]. The equipment of the acoustic defectoscope for pumping rods ADNH [16–18] was used to control the composite fittings. In the experiment, the shape of the echogram was evaluated. Fittings with local defects include fittings having a clear local impulse in the analyzed area (1.5–5.5 m), with a level exceeding 2 % of the value of the bottom signal.

EVALUATION OF FITTINGS USING A ROD WAVE

The groups of fittings on which the experiments were performed are given in Table 1. Missing numbers correspond to fittings whose diameter was higher than the claimed one and did not allow the sensor to be installed, which in itself is a manufacturing defect (GOST 31938-2012).

Table 1. Fittings groups from different manufacturers

Group	Color	Total	Tested	Missing numbers
No. 1	Light brown	300	238	01, 04, 07-09, 17, 26, 29, 31, 38–39, 47, 52, 58, 71–73, etc.
No. 2	Light yellow	298	269	216, 193, 191, 110, 112, 106, 191, 80, 81, 57–59, 61, 62, 45, 27
No. 3	Light yellow	300	296	194, 196, 200
No. 4	Black	150 (No. 001 – No. 150)	150	
No. 5	Black	150 (No. 151 – No. 300)	149	151
Total		1198	1105	

Fittings are divided in groups based upon manufacturers. There are 15 defective fittings were detected in the first group (that is 6.3 % of all fittings in the group), in the second – 4 (1.5 %), in the third – 18 (6.1 %), in the fourth – 0, and 2 (1.3 %) in the fifth group. The 2 % level selection is due to the average noise level for all parties.

In the diagram (Figure 2) the blue color indicates the number of fittings whose signal amplitude from the defect exceeded the level of 2 %. It also includes samples whose signal amplitude exceeded the levels of 5 % and 10 %. The pink color indicates a group of samples whose amplitude of the echo signal from the defect exceeded the level of 5 %, and also includes samples with signal amplitude exceeding the level of 10 %. Green color indicates the number of samples whose signal amplitude from the defect has exceeded the level of 10 %. The number of the group is plotted along the abscissa axis, the percentage of the number of defective samples per group is plotted along the ordinate axis.

Thus the most part of defective fittings belongs to the first group.
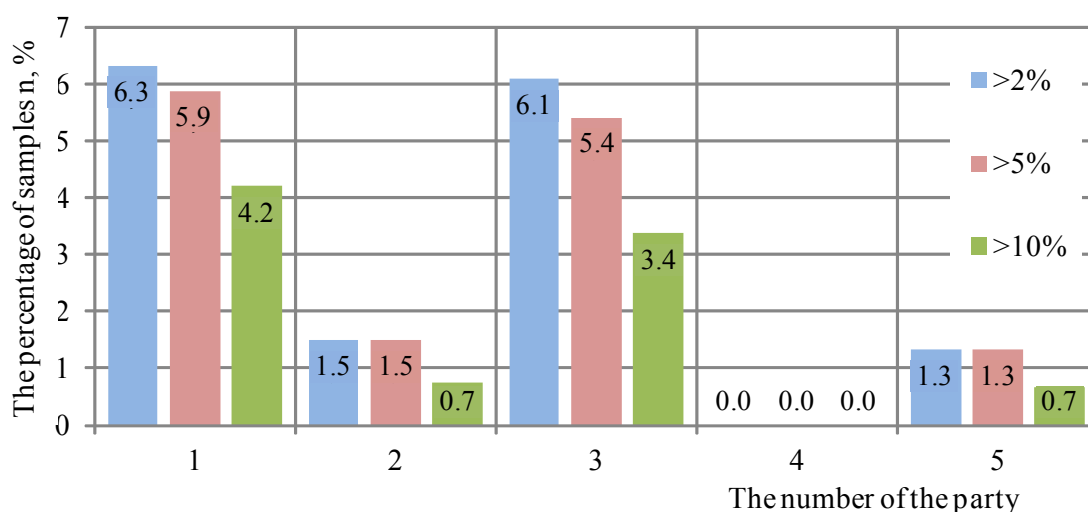
Figure 2. Composite fiberglass fittings

DEFECTOSCOPY OF COMPOSITE FIBERGLASS FITTINGS

When carrying out defectoscopy using rod waves, the amplitude of signals from local defects depends on the value of the ratio of the cross-sectional area along the entire length of the object to the cross-section area in the defect zone. In accordance with the patterns of propagation of the rod wave, the reflection from the defective zone of the waveguide is determined by the change in the mechanical impedance of the waveguide $Z = \rho C S$ (S – cross-section square, C – wave speed, ρ – density). In the simplest case, when moving from a section with a mechanical impedance Z_1 to a section with a mechanical impedance Z_2 the reflection coefficient R is defined by formula: $R = (Z_2 - Z_1) / (Z_2 + Z_1)$. If the material properties of the waveguide do not change ($C = $ const), and only its cross section changes (surface defects leading to the loss or addition of some part of the metal), R is defined by formula: $R = (S_2 - S_1) / (S_2 + S_1)$ [19–20]. This makes it possible to evaluate the interaction of acoustic waves with defects that weaken the cross-section of the object: captives, weights, inclusions, rubs, delaminations, etc. For defects that are concentrators of mechanical stresses (cracks with small opening) that do not significantly change the mechanical impedance of the object, the mechanism of emission of acoustic emission waves from regions where the stress exceed the mean value over the

cross section of the monitoring object during the passage of the probe impulse (stretching-compression) works.

The examined samples (Table 2) are located depending on the magnitude of the signal level from the local defect, expressed as a percentage of the 1st bottom impulse and calculated by the formula:

$$A = U_D / U_{Don} \cdot 100\ \%, \tag{1}$$

where U_{Don} – amplitude of the first bottom signal; U_D – amplitude of the first defect signal.

The defects are modeled in the Compass 3D solid modeling software environment. The coefficients of the square change in the area of sections of local defects ("area ratios") were calculated by formula:

$$K_S = S_0 / S_d \cdot 100\ \%, \tag{2}$$

where S_0 – square of the flawless area; S_d – square of the defect area.

Among the defects of tested fittings with measured cross-sectional squares, the node defects were 22.2 %, defects of the inflow type were 44.4 %, defects of the gap type were 22.2 %, defects of the thickening type were 5.5 %, defects of the delamination type amounted to 5.5 %.

Table 2. Dependence of the reflection ratio on the size of the defects

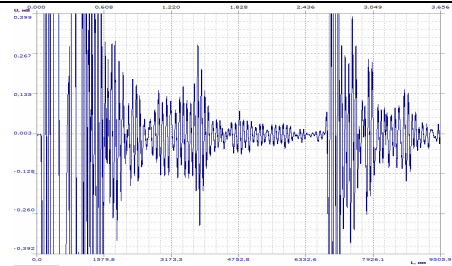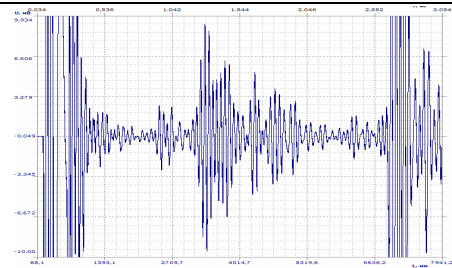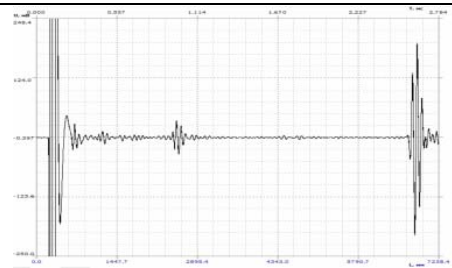| No.	Sample	The reflection ratio R	Area ratio K_s, %	The nature of the defect
1	3-072	2.8	11.1	node
2	1-148	4.0	1.0	node
3	3-089	5.9	8.7	node
4	2-254	6.9	7.7	inflow
5	1-003	7.3	6.9	inflow
6	4-201	7.7	4.4	gap
7	3-045	9.4	26.3	inflow
8	2-219	10.5	23.5	gap
9	4-300	10.8	9.25	gap
10	1-263	12.0	10.2	node
11	1-260	12.1	26.8	inflow
12	1-013	12.2	21.3	delamination
13	3-249	12.7	3.2	thickening
14	1-059	14.8	32.1	inflow
15	1-151	15.8	37.5	node inflow
16	1-280	17.2	12.0	node inflow
17	3-047	21.0	40.9	thickening
18	3-273	21.5	31.8	inflow

A graphical dependence of the amplitude of the signal on the defect on the value of the square of the defect area is obtained (Figure 3).

Analysis of the graphical dependence showed that there are "fall out" points marked red and green. Red color indicates points that, with a relatively small sectional area of the local defect, give a large defect signal magnitude. This is because the defect is mainly determined by the destruction of the fitting body and is visible on the surface. The points marked green give a smaller defect signal magnitude from the defect. Such samples and their sizes are presented in Table 3.
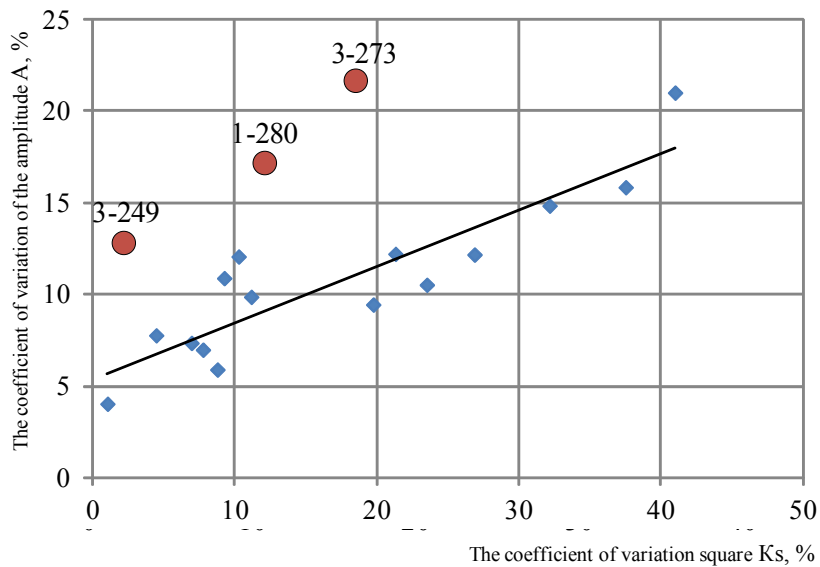
Figure 3. Dependence of amplitudes to defects squares

Table 3. Defects types and sizes

View of the defect	Echogram
Sample number / Defect size, mm / Defect type	
3-249 / 13x9 / Thickening	
3-273 / 6x13/ Inflow	
1-280 / 10x13/ Node	

Defects 3-249, 1-280, 3-273 on the echogram are expressed by a large signal, probably due to not visible internal breaking of the section.

CONCLUSION

Acoustic guided wave testing is applicable for composite fiberglass fittings defectoscopy with the use of a rejection level of 2 %.

The main types of defects detected are: a deficiency or excess of epoxy resin (44 %), delamination (5.5 %), fiberglass thread breakage (22 %).

Along with the apparent dependence between the size of the defect and the amplitude of the echo signal from the defect, samples that "fall out" of this dependence are found, characterized by the presence of internal defects. The percentage of such "fall out" samples was 16 %.

The technology of production of composite fittings assumes the obligatory restoration of the fiberglass thread breakage, while the technological process stops, which is determined by the defectoscope. For the case of responsible use of armature, the removal of fragments with such defects must be mandatory and unimportant in case of domestic use.

REFERENCES

1. Grakhov, V. P., & Saidova, Z. S. (2017). Technique for determining the degree of cure in composite polymer reinforcements. *Intelligent Systems in Manufacturing, 15*(1), 96–98. doi:10.22213/2410-9304-2017-1-96-98.

2. Murashov, V. V., & Generalov, A. S. (2014). Testing of multilayer adhesive structures using low-frequency acoustics methods. *Aviation Materials and Technologies, 31*(2), 59–67.

3. Klyuev, V. V. (Ed.). (2006). *Non-destructive testing. Reference book in 8 volumes.* Moscow, Russia: Spektr.

4. Bergmann, L. (1954). *Der ultraschall und seine anwendung in wissenschaft und technik [Ultrasound and its application in science and technology]*. Stuttgart: Hirzel. (in German).

5. Trifonova, S. I., Generalov, A. S., & Dalin, M. A. (2017). Sovremennyye tekhnologii i sredstva tenevogo ul'trazvukovogo kontrolya polimernykh kompozitsionnykh materialov [Modern technologies and means of shadow ultrasonic testing of polymeric composite materials]. *Tekhnologiya Mashinostroeniya [Mechanical-Engineering Technology], 2017*(7), 37–43 (in Russian).

6. Murav'eva, O. V., Murav'ev, V. V., Strizhak, V. A., Murashov, S. A., & Pryakhin, A. V. (2017). *Akusticheskiy volnovodnyy kontrol' lineyno-protyazhennykh ob"yektov [Acoustic guided wave testing of linearly extended objects]*. Novosibirsk, Russia: SB RAS Publ. (in Russian). ISBN 978-5-7692-1560-5.

7. Budenkov, G. A., Nedzvetskaya, O. V., Zlobin, D. V., & Lebedeva, T. N. (2004). The application efficiency of rod and torsional waves for checking rod-shaped roll stock. *Russian Journal of Nondestructive Testing, 40*(3), 147–151. doi:10.1023/B:RUNT.0000040171.56679.6b.

8. Murav'eva, O. V., Murashov, S. A., & Len'kov, S. V. (2016). Torsional waves excited by electromagnetic–acoustic transducers during guided-wave acoustic inspection of pipelines. *Acoustical Physics, 62*(1), 117–124.

9. Murav'eva, O. V., & Zlobin, D. V. (2013). The acoustic path in the method of multiple reflections during nondestructive testing of linearly extended objects. *Russian Journal of Nondestructive Testing, 49*(2), 93–99. doi:10.1134/S1061830913020058.

10. Murav'eva, O. V., Len'kov, S. V., Murav'ev, V. V., Myshkin, Y. V., & Murashov, S. A. (2016). Factors that affect the excitation effectiveness of torsional waves during waveguide inspection of pipes. *Russian Journal of Nondestructive Testing, 52*(2), 78–84. doi:10.1134/S1061830916020066.

11. Myshkin, Yu. V., & Muraveva, O. V. (2017). The features of the guided wave excitation and propagation at testing of pipes. *Journal of Physics: Conference Series, 881*(1), 012019. doi:10.1088/1742-6596/881/1/012019.

12. Muraveva, O. V., Myshkin, Y. V., & Lenkov, S. V. (2016). Factors affecting attenuation of torsional waves in pipes loaded on contact viscoelastic media. *Russian Journal of Nondestructive Testing, 52*(9), 485–491. doi: 10.1134/S1061830916090035.

13. Murav'ev, V. V., Murav'eva, O. V., Strizhak, V. A., Pryakhin, A. V., & Fokeeva, E. N. (2014). An analysis of the comparative reliability of acoustic testing methods of bar stock from spring steels. *Russian Journal of Nondestructive Testing, 50*(8), 435–442. doi:10.1134/S1061830914080063.

14. Budenkov, G. A., Korobeinikova, O. V., Kokorin, N. A., & Strizhak, V. A. (2007). Opyt priemochnogo akusticheskogo kontrolya i uprochneniya nasosnykh shtang pri servisnom obsluzhivanii [Experience of acceptance acoustic control and hardening of pump rods at the time of maintenance service]. *V mire nerazrushayushchego kontrolya [NDT World],* 2007(4), 14–19 (in Russian).

15. Murav'eva, O. V., Strizhak, V. A., Zlobin, D. V., Murashov, S. A., Pryakhin, A. V., & Myshkin, Yu. V. (2016). Acoustic waveguide testing of downhole pumping equipment elements. *Oil Industry, 2016*(9), 110–115.

16. Strizhak, V. A., Pryakhin, A. V., Khasanov, R. R., & Efremov, A. B. (2017). Hardware-software complex for rods control by mirror-shadow method using multiple reflections. *Journal of Instrument Engineering, 60*(6), 173–178 (in Russian). doi: 10.17586/0021-3454-2017-60-6-565-571.

17. Muraviev, V. V., Strizhak, V. A., & Hasanov, R. R. (2016). Features of the software for the hardware-based system of acoustic tensometry and structural inspection of metal products. *Intelligent Systems in Manufacturing, 14*(2), 71–75 (in Russian).

18. Murav'eva, O. V., Strizhak, V. A., Zlobin, D. V., Murashov, S. A., & Pryakhin, A. V. (2014). Tekhnologiya akusticheskogo volnovodnogo kontrolya nasosno-kompressornykh trub [Technology of acoustic waveguide inspection of pumping and compression pipes]. *V mire nerazrushayushchego kontrolya [NDT World], 66*(4), 51–56 (in Russian).

19. Budenkov, G. A., & Nedzvetskaya, O. V. (2004). Principal regularities of Pochhammer-wave interaction with defects. *Russian Journal of Nondestructive Testing, 40*(2), 99–108. doi: 10.1023/B:RUNT.0000036552.46582.a0.

20. Muraveva, O. V., Strizhak, V. A., & Pryakhin, A. V. (2014). The effect of regular differences in a cross section on the testability of a rod tested by the acoustic waveguide method. *Russian Journal of Nondestructive Testing, 50*(4), 219–226. doi:10.1134/S1061830914040068.

21. Budenkov, G. A., Nedzvetskaya, O. V., Zlobin, D. V., & Murashov, S. A. (2006). Interaction of torsion waves with longitudinal cracks in tubes. *Russian Journal of Nondestructive Testing, 42*(6), 392–397. doi:10.1134/S1061830906060064.